OKLAHOMA TRANSPORTATION CENTER

ECONOMIC ENHANCEMENT THROUGH INFRASTRUCTURE STEWARDSHIP

REAL TIME ASSESSMENT OF DYNAMIC LOADS ON BRIDGES

THORDUR RUNOLFSSON, PH.D.
ASISH MADHAVARAM, M.SC.

OTCREOS11.1-54-F

Oklahoma Transportation Center
2601 Liberty Parkway, Suite 110
Midwest City, Oklahoma 73110

Phone: 405.732.6580
Fax: 405.732.6586
www.oktc.org

DISCLAIMER

The contents of this report reflect the views of the authors, who are responsible for the facts and accuracy of the information presented herein. This document is disseminated under the sponsorship of the Department of Transportation University Transportation Centers Program, in the interest of information exchange. The U.S. Government assumes no liability for the contents or use thereof.

TECHNICAL REPORT DOCUMENTATION PAGE

1. REPORT NO.	2. GOVERNMENT ACCESSION NO.	3. RECIPIENTS CATALOG NO.
OTCREOS11.1-54-F		

4. TITLE AND SUBTITLE	5. REPORT DATE
Real Time Assessment of Dynamic Loads on Bridges	May 30, 2013
	6. PERFORMING ORGANIZATION CODE
7. AUTHOR(S)	8. PERFORMING ORGANIZATION REPORT
Thordur Runolfsson, Asish Madhavaram	
9. PERFORMING ORGANIZATION NAME AND ADDRESS	10. WORK UNIT NO.
School of Electrical and Computer Engineering The University of Oklahoma 110 W Boyd St, Norman, OK 73019	11. CONTRACT OR GRANT NO. DTRT06-G-0016
12. SPONSORING AGENCY NAME AND ADDRESS	13. TYPE OF REPORT AND PERIOD COVERED
Oklahoma Transportation Center (Fiscal) 201 ATRC Stillwater, OK 74078 (Technical) 2601 Liberty Parkway, Suite 110 Midwest City, OK 73110	Final, 10/1/2011-5/31/2013
	14. SPONSORING AGENCY CODE

15. SUPPLEMENTARY NOTES

University Transportation Center

16. ABSTRACT

Highway bridges are an important class of civil structures that are subject to continuously acting and varying dynamic loads due to traffic. A large number of highway bridges in the US (bridges on interstate highways or state highways which have high speed limits) were built about 50 years ago and are approaching critical age in terms of deterioration and may be in need of maintenance and/or replacement. Consequently, the need for advanced methods of highway bridge health monitoring, damage detection and estimation of load patterns has reached a critical stage. With recent advances in sensor and network technologies, it has become possible to instrument structures with embedded sensors that continuously measure the dynamic response of the structure, which is the combined response of the bridge and vehicle loads. In this project, we developed a technique for data driven real time estimation of the dynamic loads generated by vehicles passing on bridge structures. The approach is based on robust optimal feedback control ideas and uses a simplified gray box model for the bridge that has been identified using multiple sets of sensor data. Robustness of the developed approach against modeling uncertainties is demonstrated.

17. KEY WORDS	18. DISTRIBUTION STATEMENT		
Highway bridges, dynamic loads, load estimation	No restrictions. This publication is available atwww.oktc.org and from NTIS.		
19. SECURITY CLASSIF. (OF THIS REPORT)	20. SECURITY CLASSIF. (OF THIS PAGE)	21. NO. OF PAGES	22. PRICE
Unclassified	Unclassified	58 + covers	

SI (METRIC) CONVERSION FACTORS

Approximate Conversions to SI Units

Symbol	When you know	Multiply by	To Find	Symbol
	LENGTH			
in	inches	25.40	millimeters	mm
ft	feet	0.3048	meters	m
yd	yards	0.9144	meters	m
mi	miles	1.609	kilometers	km
	AREA			
in^2	square inches	645.2	square millimeters	mm
ft^2	square feet	0.0929	square meters	m^2
yd^2	square yards	0.8361	square meters	m^2
ac	acres	0.4047	hectares	ha
mi^2	square miles	2.590	square kilometers	km^2
	VOLUME			
fl oz	fluid ounces	29.57	milliliters	mL
gal	gallons	3.785	liters	L
ft^3	cubic feet	0.0283	cubic meters	m^3
yd^3	cubic yards	0.7645	cubic meters	m^3
	MASS			
oz	ounces	28.35	grams	g
lb	pounds	0.4536	kilograms	kg
T	short tons (2000 lb)	0.907	megagrams	Mg
	TEMPERATURE (exact)			
°F	degrees Fahrenheit	(°F-32)/1.8	degrees Celsius	°C
	FORCE and PRESSURE or STRESS			
lbf	poundforce	4.448	Newtons	N
lbf/in^2	poundforce per square inch	6.895	kilopascals	kPa

Approximate Conversions from SI Units

Symbol	When you know	Multiply by	To Find	Symbol
	LENGTH			
mm	millimeters	0.0394	inches	in
m	meters	3.281	feet	ft
m	meters	1.094	yards	yd
km	kilometers	0.6214	miles	mi
	AREA			
mm^2	square millimeters	0.00155	square inches	in^2
m^2	square meters	10.764	square feet	ft^2
m^2	square meters	1.196	square yards	yd^2
ha	hectares	2.471	acres	ac
km^2	square kilometers	0.3861	square miles	mi^2
	VOLUME			
mL	milliliters	0.0338	fluid ounces	fl oz
L	liters	0.2642	gallons	gal
m^3	cubic meters	35.315	cubic feet	ft^3
m^3	cubic meters	1.308	cubic yards	yd^3
	MASS			
g	grams	0.0353	ounces	oz
kg	kilograms	2.205	pounds	lb
Mg	megagrams	1.1023	short tons (2000 lb)	T
	TEMPERATURE (exact)			
°C	degrees Celsius	9/5+32	degrees Fahrenheit	°F
	FORCE and PRESSURE or STRESS			
N	Newtons	0.2248	poundforce	lbf
kPa	kilopascals	0.1450	poundforce per square inch	lbf/in^2

REAL TIME ASSESSMENT OF DYNAMIC LOADS ON BRIDGES

FINAL REPORT

May 2013

Thordur Runolfsson, Ph.D.
Professor and Associate Director
School of Electrical and Computer Engineering

Asish Madhavaram, M.Sc.
Research Associate
School of Electrical and Computer Engineering

The University of Oklahoma
Norman, OK 73019

Oklahoma Transportation Center
2601 Liberty Parkway, Suite 110
Midwest City, Oklahoma 73110

Table of Contents

List of Figures

Executive Summary

Highway bridges are an important class of civil structures that are subject to continuously acting and varying dynamic loads due to traffic. A large number of highway bridges in the US (bridges on interstate highways or state highways which have high speed limits) were built about 50 years ago and are approaching critical age in terms of deterioration and may be in need of maintenance and/or replacement. Consequently, the need for advanced methods of highway bridge health monitoring, damage detection and estimation of load patterns has reached a critical stage. With recent advances in sensor and network technologies, it has become possible to instrument structures with embedded sensors that continuously measure the dynamic response of the structure, which is the combined response of the bridge and vehicle loads. In this project, we developed a technique for data driven real time estimation of the dynamic loads generated by vehicles passing on bridge structures. The approach is based on robust optimal feedback control ideas and uses a simplified gray box model for the bridge that has been identified using multiple sets of bridge sensor data for the Canadian River Bridge in Norman, OK. Robustness of the developed approach against modeling uncertainties, such as variations in bridge parameters due to material and environmental conditions, is demonstrated.

Chapter 1: Introduction

Structural Health Monitoring is an active field of research for premature failure detection of structures due to overloading, deterioration, etc. Highway Bridges are an important class of civil structures, which are subject to continuously acting and varying dynamic loads due to traffic. Many highway bridges are steel and concrete bridges, which are usually constructed with a design life of between 50 and 100 years. In the US, many highway bridges are more than 50 years old and are approaching critical age in terms of structural deterioration and need for maintenance/replacement. Consequently, the need for advanced methods for health monitoring, damage control and estimation of load patterns has reached a critical stage. Traditional methods for structural health monitoring have been limited to visual inspection and manually applied nondestructive measurements based on acoustic, x-ray, magnetic field and other measurement techniques [6], [10]. With recent improvements in sensor and network technologies [3], [4], it has become possible to instrument structures with embedded sensors that continuously measure the dynamic response of the structure. Such measuring devices (sensors) are particularly important in monitoring the health of civil structures such as bridges that are subjected to continuously varying loads.

Extensive studies have been made in using such measurements to identify the dynamics of bridge structures and research efforts in using these measurements for structural health monitoring are ongoing [4], [13], [10], [8]. The developed methods use a variety of model identification techniques such as ARMA (Auto regressive moving average model) and State Space model identification [10]. Identified models and their change over time are then used in combination with extensive computer based analysis to access the health of the structure. For bridges, the measured response is the combined response of the bridge and the vehicle loads and assumptions are made about the nature of the vehicle load. In most of the cases vehicle effect is minimal on the overall bridge model because the vehicles are much lighter than the bridge structure. When these assumptions are not valid, the identified models can have considerable errors and the results of model based analysis have significant uncertainty. In particular, a variation in the modal frequencies is observed as well as mode shapes (shapes defined by motion of two or more points on a structure) are detected that do not fit model assumptions and do not have clear structural meaning.

In this project, we have developed techniques for a data driven real time estimation of the dynamic loads generated by vehicles travelling on bridge structures. Some conventional estimation techniques, such as Kalman filtering are not well suited for the estimation of the vehicle loads because such techniques require a model of the vehicles to generate the loads and model of the vehicles are continuously changing in time due to changes in traffic, which is too fast for the utilization of adaptive estimation techniques. Consequently, in this research, we developed a novel alternative approach where no dynamic model of the load is required and the input load is estimated directly. Estimating the input to a dynamic system is a system inversion problem that is generally not well posed. Consequently, an approximate inversion problem was solved. We developed a physics based reduced order bridge model (Gray box model) using the bridge response data.

This research enables the real time estimation of vehicle loads. The approach is based on a novel combination of techniques from physics based modeling, model reduction, data driven model identification and control theory. This research is the continuation of the bridge identification work in Dynamic Structural Sensing and Control Center (DySSC) at the University of Oklahoma and utilized bridge response data from the Canadian River Bridge in Norman, OK. The continuation of this work will involve utilizing the new high fidelity sensor network that is being installed on the Canadian River Bridge in Norman, OK as well as field testing of the developed techniques.

2.1 Review of Existing Models

The problem of identifying the input force affecting a structure has received a considerable attention in the literature. Most of the existing techniques are time domain methods and employ some kind of optimization for the approximate inversion of the system dynamics. Frequently the problem is considered in discrete time i.e. a linear time invariant system of the form

$$\begin{aligned} x_{k+1} &= Ax_k + Bu_k \\ y_k &= Cx_k + Du_k \end{aligned} \qquad (0.0)$$

where x_k is the state, y_k is the measured output and u_k is the unknown input. The objective is to reconstruct or estimate the system input based on the measured output, assuming that the systems matrices (A, B, C, D) are known. Frequently the system and output (measurement) equations are corrupted by noise as well. The problem of reconstructing the state x_k from the measured past input $(y_0, ..., y_k)$ is a standard filtering or estimation problem and can be solved using traditional estimation techniques where the objective is to minimize an error criteria for the state estimation error. A similar idea is used for the estimation or reconstruction of the input sequence u_k in several publications. In [9] the authors write the solution of (2.1) in the standard form.

$$y_k = h_k^0 x_0 + \sum_{i=0}^{k} h_i u_{k-i}$$

where $h_i = CA^i B + D\delta_i$ (δ_i is the unit impulse) are the Markov parameters and $h_i^0 = CA^i, i = 0, ...$ Assuming that the initial condition is known and writing the response

$$\hat{y}_k = y_k - h_k^0 x_0 = \sum_{i=0}^{k} h_i u_{k-i} \text{ for } k = 0, ..., N$$

This results in a matrix equation relating $\hat{y}_k, k = 0, ..., N$ to $u_k, k = 0, ..., N$. The solution of this equation (minimizing a least squares criteria) under various conditions is studied in detail in

[9]. An alternative approach is considered in [12] where the authors consider an approach based on a direct model of the inverse dynamics of (2.1) and construct a so-called Inverse Structural Filter (ISF) of the form

$$u_k = \sum_{i=0}^{N_R-1} r_i y_{k-i+1}$$

The parameters r_i, the ISF weights, are obtained by solving an associated matrix inversion problem. The approaches in [9] and [12] are mathematically similar but some differences in the resulting filter weights.

An alternative approach is considered in [3] where the bridge (structure) is modeled as a simply supported beam of the form (2.8) and an expansion of the solution of this equation is used to construct a set of matrix equations relating the vertical displacement and the input force (which also has an assumed simple form). The resulting matrix equation is then solved for the input force. In all of the above approaches the problem that is solved is an (open loop) optimization problem that grows in size with time. Consequently, an approximate solution that truncates the size of the problem has to be considered in a practical problem. Furthermore, in these approaches it is assumed that the initial condition is known. An alternative approach is to consider the inversion problem as a closed loop (feedback) problem. In such formulation, the "size" of the problem is determined by the system dimensions and is independent of the length of the time history. Additionally, a feedback configuration is robust to uncertainty in model parameters and can be designed to reject the effects of external unknown disturbances. Guided by these principles we will design a feedback system for the estimation of the unknown systems loads.

2.2 H - infinity Control Design

H_∞ (H - infinity) control is a method for designing controllers for time invariant control systems that achieves robust performance [1]. Various control performance objectives can be formulated as a H_∞ control problem. In our research, we employ H_∞ control for loop-shaping, where we shape the closed loop transfer function of the system to meet performance and robustness specifications. In H_∞ design, the performance specifications are made in the frequency-

domain. H_∞ control design is frequently performed iteratively, i.e. weights of the performance function are modified iteratively until desired performance is obtained [14].

To illustrate the basic concept of H_∞ control consider the single loop feedback system in Figure 2. Let $F(s)$ be a function of the complex variable s. Assume $F(s)$ is analytic and bounded in open right half plane, i.e. $|F(s)| \le b, \quad \text{Re } s > 0$. The least such bound b is the H_∞ norm of F, denoted by

$$\|F\|_\infty := \sup\{|F(s)| : \text{Re } s > 0\} \tag{0.0}$$

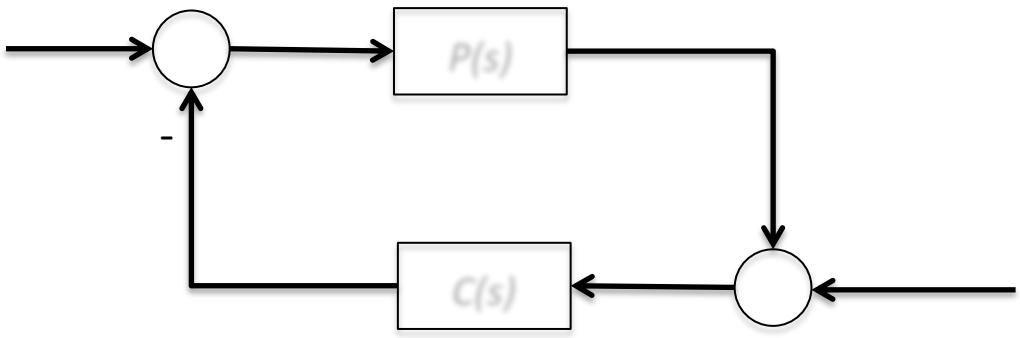

Figure 2.1 Single-Loop feedback system. The plant is characterized by P(s) and the controller by C(s). v_1 and v_2 are external inputs and u_1 and u_2 are error signals.

The transfer functions $P(s)$ and $C(s)$ in Figure 2.1 are transfer functions assumed to be strictly proper, real-rational and stable. Due to the assumptions on P and C, the feedback system is internally stable if the closed loop transfer functions from v_1 and v_2 to u_1 and u_2 are all stable. According to Nyquist Criterion feedback system is internally stable if and only if the Nyquist plot of PC doesn't pass through or encircle the point $s = 1$. So feedback system is internally stable if $\|PC\|_\infty < 1$ [1].

2.2.1 Stability criteria for H-infinity control design

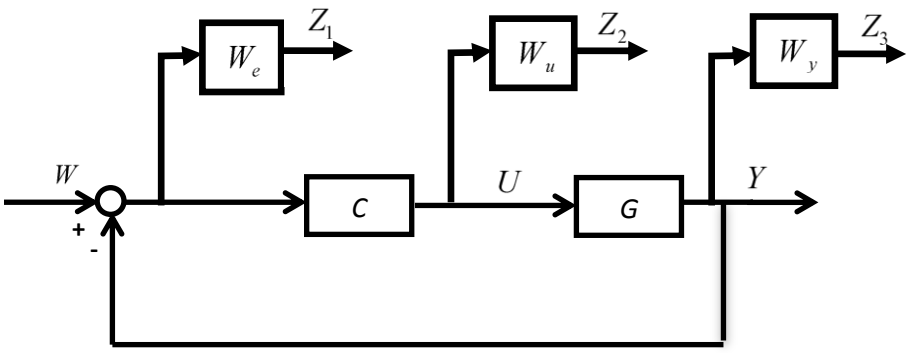

Figure 2.2 Mixed Sensitivity S/R/T design. G is the plant, C is the controller, the W's are design weights for the sensitivity function, control sensitivity function and complementary sensitivity function.

Consider a standard mixed sensitivity S/R/T design [17] shown in Figure 2.2. Here, C is the controller, G is the plant, $W_e(s)$, $W_u(s)$ and $W_y(s)$ are the weights for the sensitivity function $S(s)$, the control signal sensitivity function $R(s)$, and the complimentary sensitivity function $T(s)$ respectively where

$$\begin{aligned} S &= (1+GC)^{-1} \\ R &= CS \\ T &= GC(1+GC)^{-1} \\ S+T &= 1 \end{aligned} \tag{0.0}$$

The stability condition of the mixed sensitivity $S/R/T$ design is

$$\left\| F(P,C) \right\|_\infty = \left\| \begin{matrix} W_e S \\ W_u R \\ W_y T \end{matrix} \right\|_\infty < 1 \tag{0.0}$$

To achieve the performance and stability design requirements for a closed loop system, the major challenge in H_∞ control design is the selection of weighting functions. The controller design is strongly depended on the weights. There is no certain formula of selecting the weighting functions and they are usually determined iteratively.

2.2.2 Selection of performance weighting function W_e

From (2.4) we have $\|W_e S\|_\infty < 1$ and from (2.2) we get

$$|W_e(j\omega)S(j\omega)| \le \sup|W_e(j\omega)S(j\omega)|$$

Thus,

$$|W_e(j\omega)||S(j\omega)| < 1$$

$$|S(j\omega)| < \frac{1}{|W_e(j\omega)|} \qquad (0.0)$$

For tracking performance, we want $|S(j\omega)|$ to be small over the frequency range $[0, \omega_1]$. If we want $|S(j\omega)| < \varepsilon$ for $\omega \in [0, \omega_1]$ we pick $1/|W_e(j\omega)| < \varepsilon$ for $\omega \in [0, \omega_1]$ which is nothing but $|W_e(j\omega)| > 1/\varepsilon$ for the same $\omega \in [0, \omega_1]$. $W_e(j\omega)$ is selected to have the same number of poles and zeros. Thus, we pick a zero at a very large frequency $z_1 \approx \omega_1$.

Thus,

$$W_e(s) = K\frac{s + z_1}{s + p_1} \qquad (0.0)$$

For small ω i.e., $\omega < \omega_1, W_e(j\omega)$ will be

$$W_e(j0) = K\frac{z_1}{p_1} = \frac{1}{\varepsilon}$$

We pick $p_1 = \omega_1$ thus,

$$W_e\ j0\ = K\frac{z_1}{\omega_1} = \frac{1}{\varepsilon}$$

Let $z_1 = 10\omega_1$ then

$$W_e\ j0\ = K\frac{10\omega_1}{\omega_1} = 10K = \frac{1}{\varepsilon}$$

Therefore,

$$K = \frac{1}{10\varepsilon} \qquad (0.0)$$

Here we do not require the Uncertainty weighting function $W_y(s)$ and controlled signal weighting function $W_u(s)$ is chosen as constant in order to guarantee the controller stable.

2.3 The Load-Bridge Dynamics Model

When a vehicle passes over a bridge, the bridge is excited by the vehicle load due to the weight of the vehicle but this excitation includes additional noise generated by the uneven surface of the bridge deck and the contact of the tires of the travelling vehicle. Furthermore, there is a coupling between the dynamics of the vehicle suspension and the bridge dynamics. The overall system is portrayed in Figure 2.3.

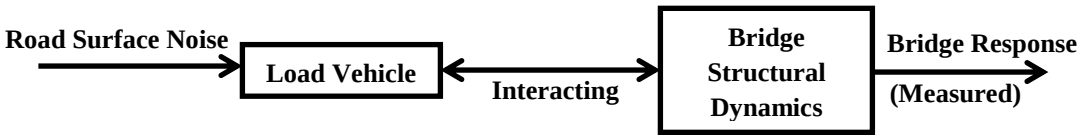

Figure 2.3 Functional Schematic of Bridge-Vehicle System from the input road surface noise to the measured bridge response.

In order to obtain a physics based mathematical model of the system in Figure 2.3, one needs to know the physical characteristics (parameters) of both the bridge (structure) as well as the load (vehicle). Furthermore, information about the roughness of the bridge deck surface is needed. While the physical parameters of the bridge are usually well known, or can be readily estimated, the parameters of the vehicles are continuously changing with the change in the traffic and consequently can at best be determined to belong to a certain range. Consequently, in many data driven modeling efforts for bridges the load characteristics are assumed to insignificant compared to the parameters of the bridge and the input to the model assumed to be white noise representing the continuously acting excitation from the road surface.

2.4 Simple Bridge Models

The simplest model for a bridge section that is subject to a moving force at constant speed is a simply supported beam shown in Figure 2.4, whose transversal dynamics are described by Bernoulli-Euler equation as

$$EJ\frac{\partial^4 v(x,t)}{\partial x^4}+\mu\frac{\partial^2 v(x,t)}{\partial t^2}+2\mu\omega_b\frac{\partial v(x,t)}{\partial t}=\delta(x-ct)P(t). \qquad (0.0)$$

Here $x\in[0,l]$ is a point along horizontal span of the beam, t is time, $v(x,t)$ is vertical displacement of the beam (measured from the rest position when the beam is loaded by its own weight), E is Young's modulus, J is the moment of inertia of the cross section, μ is the constant mass per unit length and ω_b is damping frequency of the beam. $P(t)$ is the strength of the impulse

$\delta(x-ct)$ generated by the moving load at position x when the vehicle is moving with a constant speed c.

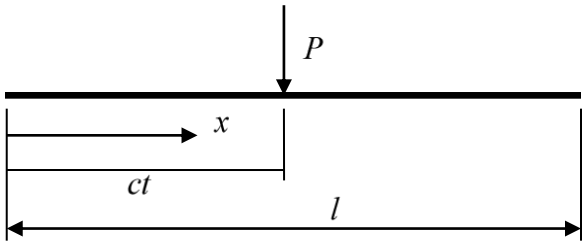

Figure 2.4 Simple beam subjected to a moving force P . l is the length of the beam, x is a point on the beam, c is speed of the moving force and t is time.

The basic assumptions made in deriving the above model are :

- The beam is of constant cross-section and constant mass per unit length.
- The mass of the moving load is small compared to the mass of the beam.
- The load moves at constant speed c starting at $x=0$ and ending at $x=l$.
- The beam damping is proportional to the velocity of vibration.

When the assumption that the mass of the moving load is small compared to the mass of the beam is not valid the above equation has to be modified to include inertial effects

$$\frac{\partial^4 v(x,t)}{\partial x^4}+\mu\frac{\partial^2 v(x,t)}{\partial t^2}+2\mu\omega_b\frac{\partial v(x,t)}{\partial t}=\delta(x-ct)\left(f(t)-\frac{d^2 v(x,ct)}{dt^2}\right) \qquad (0.0)$$

Finding an analytical solution for (2.8) for simple initial, boundary conditions and simple input forces has been studied by several authors, see e.g. the original work by [7] and the extensive analytical studies in [5]. Finding a solution of (2.9) is considerably harder but has been developing for some special cases in [5]. For the three dimensional case and more complex geometries for the bridge models it is next to impossible to find an analytical solution and numerical techniques have to be employed.

2.5 Experimental Modal Analysis

In the DySSC (Dynamic Structural Sensing and Control Center) at the University of Oklahoma, two bridges in Oklahoma have been instrumented with a network of acceleration sensors for collection of bridge response date. The data is being collected for structural health monitoring purposes as well as for real time control purposes. The sensor network on the Canadian River Bridge in Norman, Oklahoma is shown in Figure 2.5

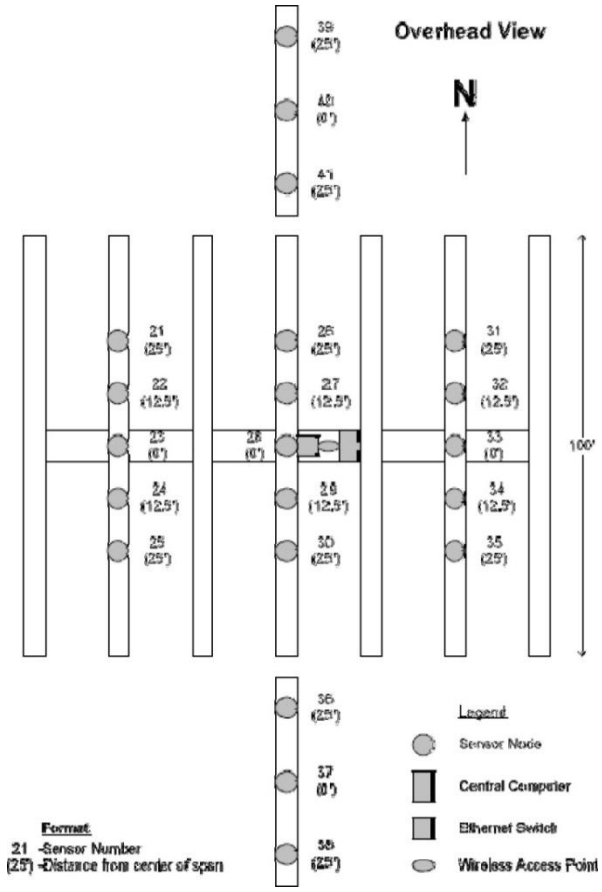

Figure 2.1 Sensor System Layout for Canadian River Bridge. The sensor locations are indicated by a gray dot.

The Canadian River Bridge is a concrete deck bridge with 38 spans and overall length of 1158 meters. Each span has a length of 30 meters. The sensor network in Figure 2.5 is located on three spans of the southbound lane of the bridge with 15 sensors on the center span and 3 sensors on each of the adjacent spans. The data collected is the vertical acceleration data of the bridge with vehicle loads on it, i.e. the systems shown in Figure 2.3. The data is recorded at a rate of 250 Hz.

A typical time history of the data collected from one of the acceleration sensor on the Canadian River Bridge is shown in Figure 2.6. We note that each peak (blob) corresponds to a different vehicle and that strength of the response due to different vehicles is quite noticeable, i.e. the weight of the vehicle is quite evident. Extensive modal analysis using this data has been carried out using various techniques and software packages.

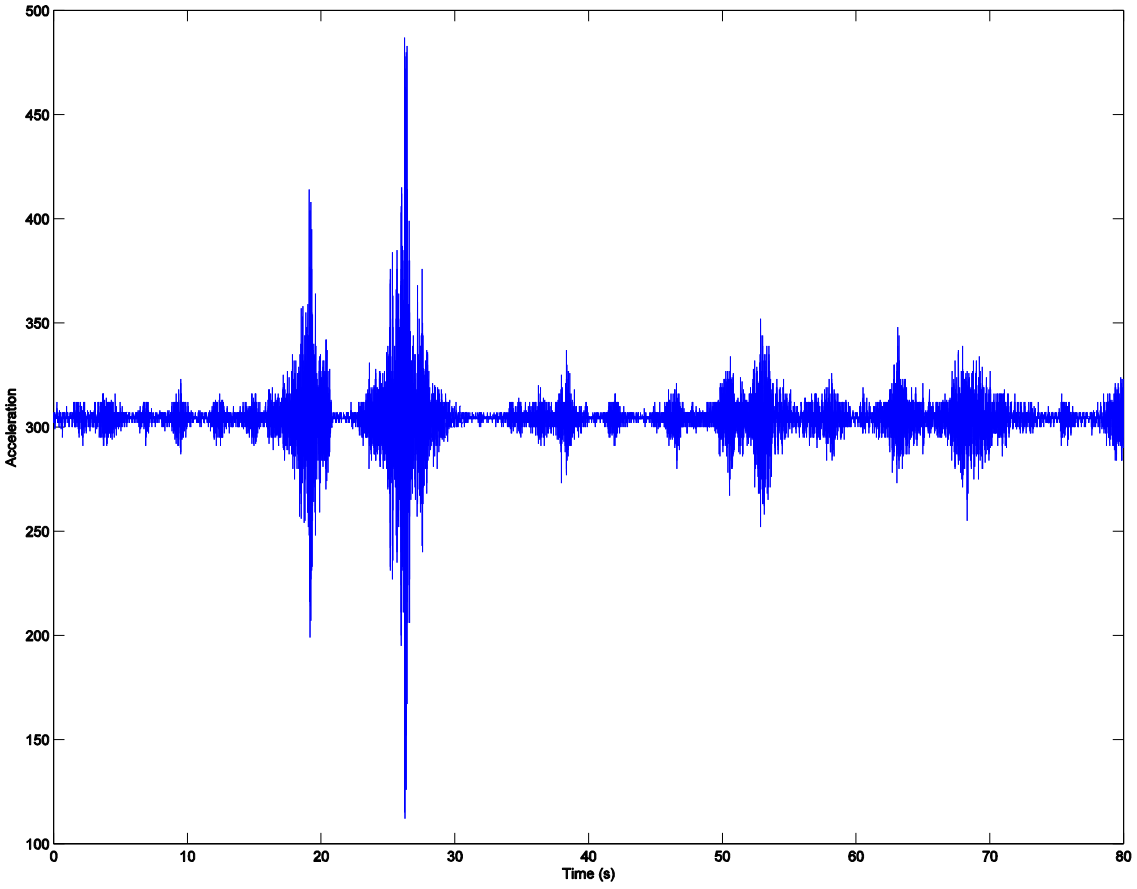

Figure 2.6 Time history snapshot from the Canadian River Bridge. Vertical acceleration is on the y-axis and time on the x-axis.

Chapter 3: Formulation of the Problem

In this section, we develop a gray box reduced order model for the beam model in (2.8). Recall the Bernoulli-Euler equation for simply supported beam

$$EJ\frac{\partial^4 v(x,t)}{\partial x^4}+\mu\frac{\partial^2 v(x,t)}{\partial t^2}+2\mu\omega_b\frac{\partial v(x,t)}{\partial t}=P(t,x) \qquad (0.0)$$

A single axle load moving at constant speed c is modeled as

$$P(t,x)=P\delta(x-ct)$$

Here

P is the magnitude of the impulse, i.e. $P=mg$ where m is the mass of the axle and g is the gravity of earth.

μ is the constant mass per unit length of the bridge.

$v(x,t)$ is the beam deflection at point x and time t

ω_b is the circular frequency of damping of the bridge

E is the Young's modulus of the bridge

J is the constant moment of inertia of the bridge cross section

l is length of the bridge section

We assume that boundary conditions are

$$\begin{aligned} &v(0,t)=0; && v(l,t)=0;\\ &\left.\frac{\partial^2 v(x,t)}{\partial x^2}\right|_{x=0}=0; && \left.\frac{\partial^2 v(x,t)}{\partial x^2}\right|_{x=l}=0, \end{aligned} \qquad (0.0)$$

i.e. the ends of the beam are fixed and for simplicity we assume the initial conditions

$$v(x,0)=0; \qquad \left.\frac{\partial v(x,t)}{\partial t}\right|_{t=0}=0 \tag{0.0}$$

Equation (3.1) together with conditions (3.2) and (3.3) can be solved using the Fourier sine integral transform and Laplace transform. First the sine transform is used to expand the spatial variable x into its harmonics, (3.1) is multiplied by $\sin j\pi x/l$ and then integrated with respect to x between 0 to l. Here, j is a mode of vibration of the simply supported beam and l is the length of the span of the bridge which is 30m in our case. We will be using following relations of Fourier sine series

$$\begin{aligned} v(x,t) &= \frac{2}{l}\sum_{j=1}^{\infty} V(j,t)\sin\frac{j\pi x}{l} \\ V(j,t) &= \int_0^l v(x,t)\sin\frac{j\pi x}{l}\,dx \end{aligned} \tag{0.0}$$

Using the boundary conditions and (3.1) we get

$$\frac{j^4\pi^4}{l^4}EJV(j,t)+m\ddot{V}(j,t)+2m\omega_b\dot{V}(j,t)=\hat{P}(j,t) \tag{0.0}$$

where

$$\hat{P}(j,t)=\int P(t,x)\sin\frac{j\pi x}{l}$$

The circular frequency (angular frequency) at the $j-$th mode of vibration of the simply supported beam is defined as

$$\omega_{(j)}^2=\frac{j^4\pi^4}{l^4}\frac{EJ}{\mu}$$

The corresponding natural frequency is

$$f_{(j)} = \frac{\omega_{(j)}}{2\pi} = \frac{j^2\pi}{2l^2}\left(\frac{EJ}{\mu}\right)^{1/2}$$

Using the above definitions, we rearrange (3.5) as

$$\ddot{V}(j,t) + 2w_b\dot{V}(j,t) + w_{(j)}^2 V(j,t) = \frac{\hat{P}(j,t)}{m}$$

Applying Laplace transformation to the above equation with $V^*(j,s) = \mathcal{L}\{V(j,t)\}$, we get

$$s^2V^*(j,s) + 2\omega_b sV^*(j,s) + \omega_{(j)}^2 V^*(j,s) = \frac{1}{\mu}\mathcal{L}(\hat{P}(j,t)).$$

Define

$$H_j(s) = \frac{1/\mu}{s^2 + 2\omega_b s + \omega_{(j)}^2},$$

then

$$V^*(j,s) = H_{(j)}(s)\mathcal{L}(\hat{P}(j,t)).$$

The index $j=1$ corresponds to the fundamental mode of the bridge. It was found in [2] that most of the energy of the bridge response is contained at the fundamental mode and thus we approximate the solution be retaining only the first term in (3.4), Therefore we obtain the approximate bridge response $v(x,t) \approx 2/l\, V(1,t)\sin \pi x/l$ where $V(1,t)$ has Laplace transform

$$V^*(1,s) = H_{(1)}(s)\mathcal{L}(\hat{P}(1,t))$$

$$\hat{P}(1,t) = P\sin\frac{\pi ct}{l} = P\sin\omega t$$

Here $T = 1/f = 2l/c$ i.e., $\omega = 2\pi f = \pi c/l$ is the circular frequency of the beam which only depends on speed of the vehicle c. We easily get $\mathcal{L}(\hat{P}(1,t)) = P\dfrac{\omega}{s^2+\omega^2}$ and thus

$$V^*(1,s) = \frac{1/\mu}{s^2 + 2\omega_b s + \omega_{(1)}^2}\frac{P\omega}{s^2+\omega^2}$$

The inverse Laplace transform gives

$$V(1,t) = v_0 \frac{1}{(1-\alpha^2)^2 + 4\alpha^2\beta^2}((1-\alpha^2)\sin\omega t - \frac{\alpha\left[\left(1-\alpha^2\right)-2\beta^2\right]}{(1-\beta^2)^{1/2}} e^{-\omega_b t}\sin\omega_{(1)}^{'} t - 2\alpha\beta(\cos wt - e^{-\omega_b t}\cos\omega_{(1)}^{'} t))$$

Where,

$\alpha = \dfrac{\omega}{\omega_{(1)}} = \dfrac{c}{2f_{(1)}l}$ is a dimensionless parameter characterizing the effect of vehicle speed

$\beta = \dfrac{\omega_b}{\omega_1}$ is another dimensionless parameter characterizing the effect of bridge/beam damping.

$v_0 = \dfrac{2Pl^3}{\pi^4 EJ} \square \dfrac{2P}{\mu l\omega_{(1)}^2}$ is the deflection at the mid-span of a beam loaded with static force P at point $x = l/2$. Let's consider a typical truck with single axle weighing 18,000Kgs. By substituting measured μ, l and $\omega_{(1)}$ of Canadian River Bridge we get $v_0 = 0.0021$ which is used in Section 3.1.

If we take central sensor location at $x = l/2$ we get

$$v\left(\frac{l}{2},t\right) \square \frac{2}{l}V(1,t) \qquad (0.0)$$

Recall that the bridge sensors measure the acceleration $\ddot{v}\left(\frac{l}{2},t\right) = \frac{2}{l}\ddot{V}(1,t)$. If we let $a(t) = \ddot{v}\left(\frac{l}{2},t\right)$ and apply Laplace transformation to $a(t)$ we get

$$\mathcal{L}\left(a(t)\right) = \frac{2}{l}s^2 H_{(1)}(s)\mathcal{L}\left(P(1,t)\right)$$

$$H(s) = \frac{2}{\mu l}\frac{s^2}{s^2 + 2\omega_b s + \omega_{(1)}^2} \qquad (0.0)$$

This is idealized transfer function of the detected system. We note that acceleration sensor has finite bandwidth and thus should be reported by a transfer function of the form $s^2/(\tau_s s+1)^2$, where $1/\tau_s$ is the sensor bandwidth.

3.1 Special Cases

Our objective is to detect the weight $P = mg$ using the measured bridge response and a measurement of the vehicle speed c . Indeed, we note that the response as given by (3.6) depends on α and β in addition to v_0 . The β depends on bridge parameters only while α depends on bridge parameters and the speed of the vehicle. Therefore, in addition to an estimate of the bridge parameters we need to know the vehicle speed and consequently, a speed detector is needed. We now consider the dynamic deflection at the center of the bridge for various values of speed (c) and damping (β).

The fundamental frequency is 3.84Hz, then

$$\omega_1 = 2\pi \times 3.84 = 24.127 \text{ rad/sec}$$

3.1.1 Static Case $c = 0$

If $c = 0$ i.e. $\alpha = 0$ and the bridge is undamped then $\omega_b = 0$ and thus $\beta = 0$, then(3.6) becomes

$$v\left(\frac{l}{2},t\right)=0$$

This means in this case there is no deflection at the mid-span of the bridge because the vehicle is immobile.

3.1.2 Case with no damping ($\beta=0$)

If the bridge is undamped then, $\omega_b=0$ and thus $\beta=0$. In this case (3.6) gives

$$v\left(\frac{l}{2},t\right)=v_0\frac{1}{1-\alpha^2}\left(\sin\omega t-\alpha\sin\omega_1 t\right)$$

The acceleration is easily found to be

$$a\left(\frac{l}{2},t\right)=v_0\frac{1}{1-\alpha^2}\left(\omega^2\sin\omega t-\alpha\omega_1^2\sin\omega_1 t\right). \qquad (0.0)$$

Consider different cases for different speeds $c=88\,km/h$ (average vehicle speed on the bridge) and $c=410\,km/h$ (very high speed which is practically impossible) with respective α values 0.108, 0.5. Figures 3.1, 3.3 shows the deflections for $c=88$ and $410\,km/h$ or $\alpha=0.108$ and 0.5 respectively.

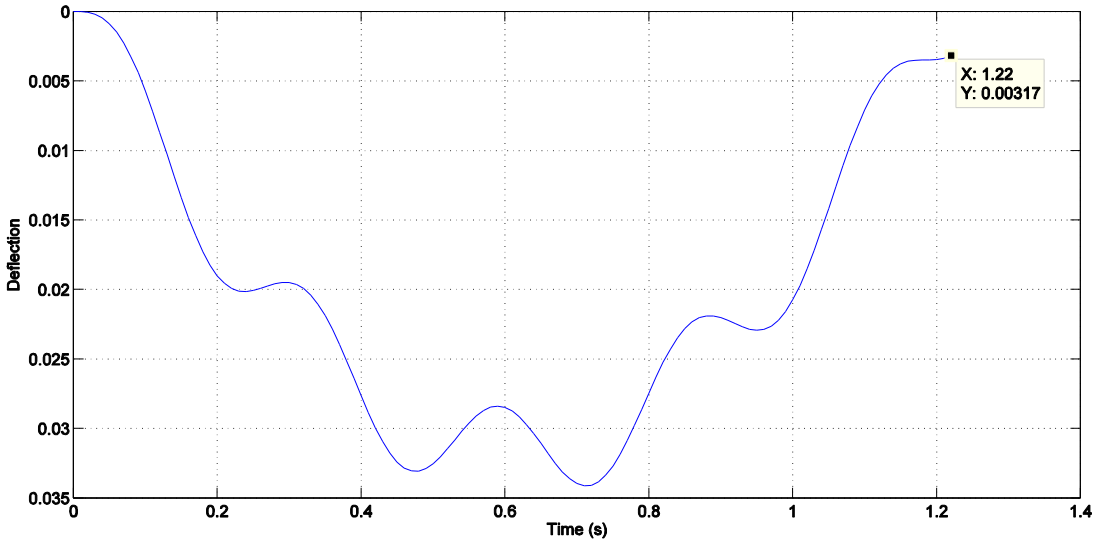

Figure 3.7 Dynamic deflection at mid-span of the bridge with $c = 88 km/h$

From Figure 3.1, when the vehicle is moving with a speed of 88 km/h we can note that the axle enters the bridge section at 0 seconds and leaves the bridge section of length 30 m at time 1.22 seconds. Here, the maximum dynamic deflection approximately occurs at the half-way of its total time on the bridge.

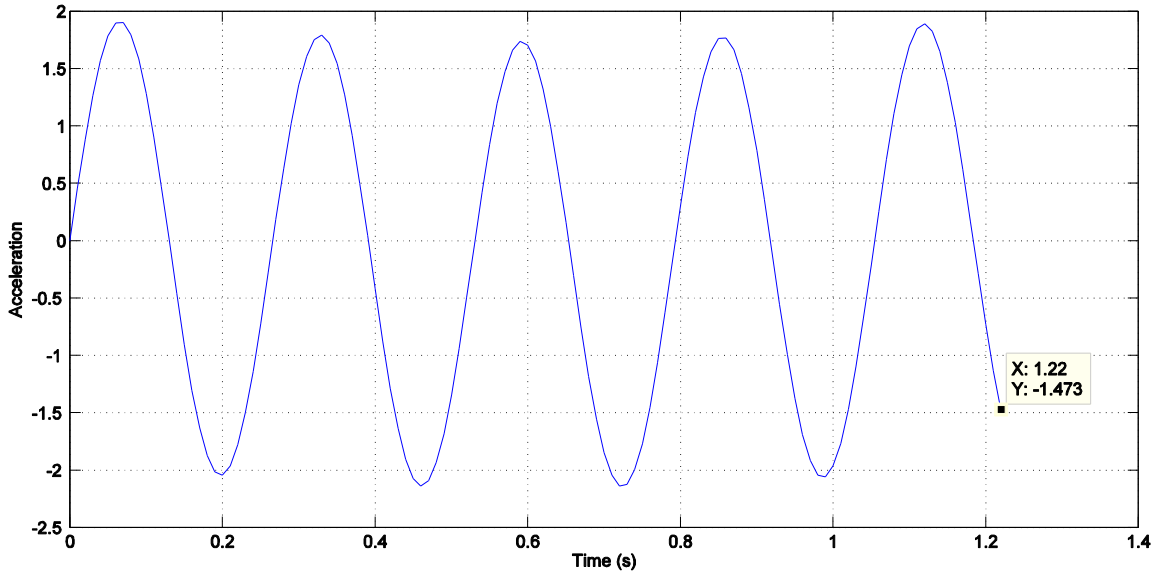

Figure 3.8 Acceleration at mid-span of the bridge with $c = 88 km/h$

Figure 3.2 is the acceleration plot of a vehicle with one axle moving at a speed of 88 km/h with a frequency of 3.8 Hz.

Figures 3.3 and 3.4 are dynamic deflection and acceleration plots of a vehicle with one axle moving with a speed of 410 km/h and we can note that the vehicle enters the span of the bridge at 0 seconds and exits at 0.26 seconds, which is much quicker than previous case because of its very high speed and the maximum deflection is more in this case and it occurs little late in the third quarter of vehicle's total time on the bridge. The acceleration plot is of the same frequency but more acceleration than at the speed 88 km/h because of its high speed.

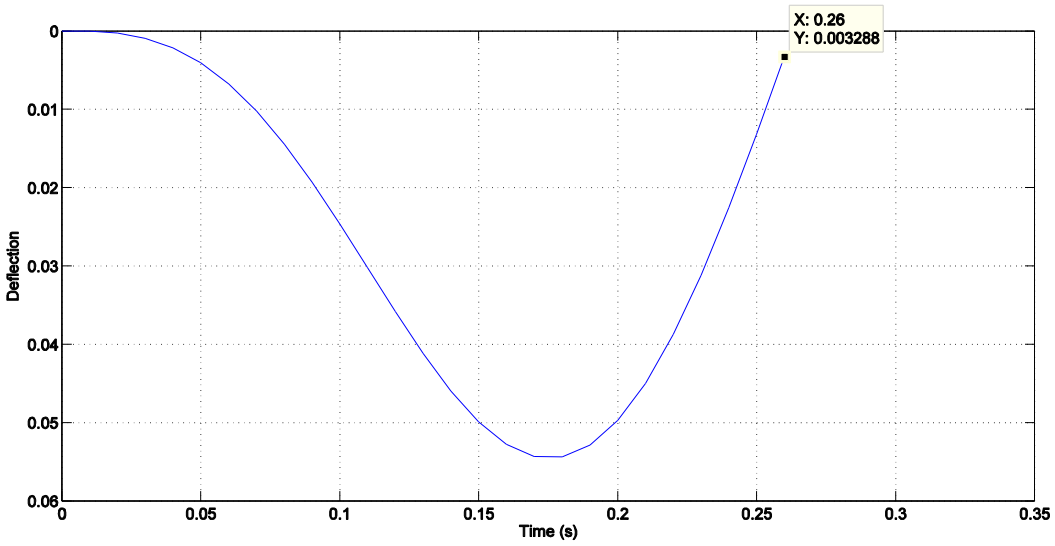

Figure 3.9 Dynamic deflection at mid-span of the bridge with $c = 410\,km/h$

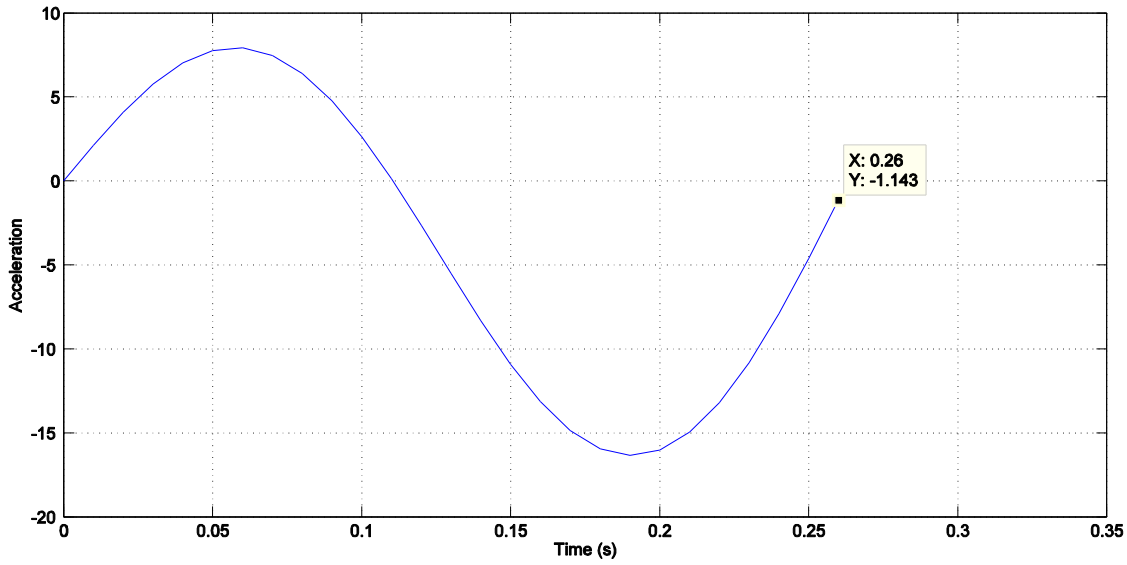

Figure 3.10 Acceleration at mid-span of the bridge with $c = 410\,km/h$

3.2 Truck with two axels

Consider a truck with two axels. Following the same load modeling as before, we model the truck as two impulse loads. Let us assume that the truck is moving with speed c and the length of the truck i.e., distance between two wheels is $\hat{l}$. Let $\hat{t}$ be the time taken by the rear wheel to cross the center of the bridge after front wheel crosses it. Then $\hat{t} = \frac{\hat{l}}{c}$ and

$$P(t,x) = P\delta(x-ct) + P\delta(x-c(t-\hat{t}))$$

$$= P\delta(x-ct) + P\delta(x-ct+\hat{l}))$$

The sine transform of the fundamental mode is

$$\hat{P}(1,t) = \int_0^l P\delta(x-ct)\sin\frac{\pi x}{l} + \int_0^l P\delta(x-ct+\hat{l})\sin\frac{\pi x}{l}$$

$$= P\sin\omega t + P\sin(\omega t - \frac{\pi\hat{l}}{l})$$

$$= P\sin\omega t + P\left(\cos\omega t\cos\frac{\pi\hat{l}}{l} + \sin\omega t\sin\frac{\pi\hat{l}}{l}\right)$$

Applying Laplace transform to $\hat{P}(1,t)$,

$$\mathcal{L}\left(\hat{P}(1,t)\right) = P\frac{\omega}{s^2+\omega^2} + P\left(\frac{s}{s^2+\omega^2}\cos\frac{\pi\hat{l}}{l} + \frac{\omega}{s^2+\omega^2}\sin\frac{\pi\hat{l}}{l}\right)$$

Therefore, $V^*(1,s) = P\left(\frac{1/\mu}{s^2+2\omega_b s+\omega_{(1)}^2}\right)\left\{\frac{\omega}{s^2+\omega^2} + \left(\frac{s}{s^2+\omega^2}\cos\frac{\pi\hat{l}}{l} + \frac{\omega}{s^2+\omega^2}\sin\frac{\pi\hat{l}}{l}\right)\right\}$

After solving the above equation and plotting it for $c = 88$ and 410 km/h or $\alpha = 0.108$ and 0.5 we get Figures 3.5 and 3.7 respectively

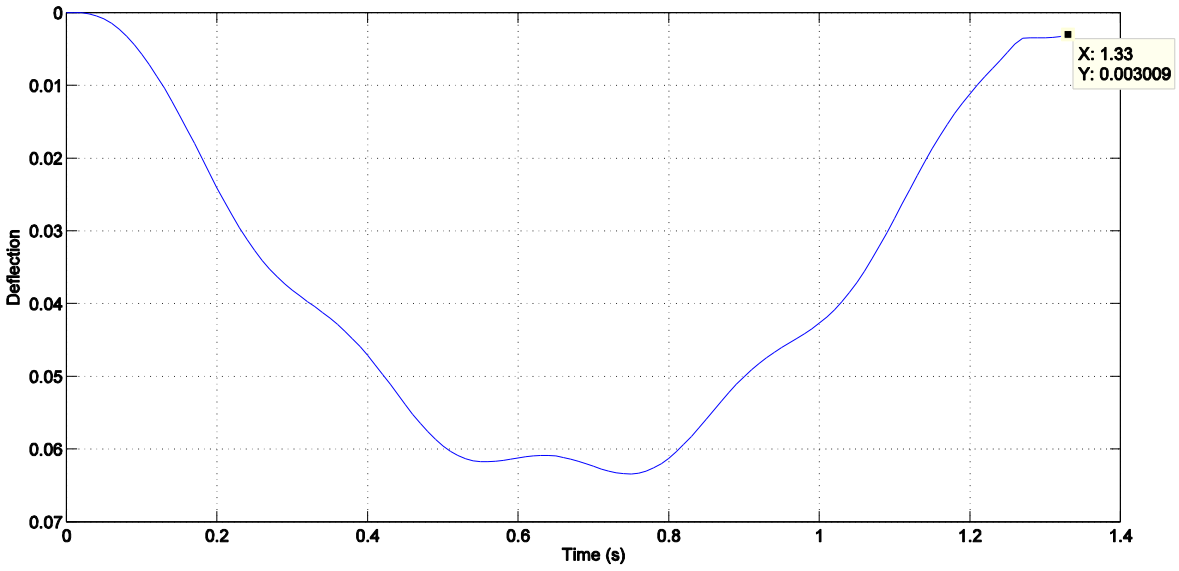

Figure 3.11 Dynamic deflection at mid-span of the bridge with $c = 88\,km/h$

From the above Figure, we can note that the first axle enters the bridge at 0 seconds and takes 1.33 seconds for the second axle to exit the bridge, which is 0.11 seconds more than the single axle vehicle. We can also note that the maximum deflection is more in this case because of the added weight, but it appears again approximately at the mid-span of its total time on the bridge.

Figure 3.6 is the acceleration plot of a two axle truck moving at a speed of 88 km/h, we can note that at 0 seconds, the first axle enters the bridge and the sensors read only the acceleration of the first axle until the second axle enters the bridge at 0.11 seconds, the first axle leaves the bridge at 1.22 seconds then we can only see the acceleration of the second axle in the Figure after 1.22 seconds until it exits the bridge at 1.33 seconds and acceleration plot have the same frequency but less acceleration when compared to the vehicle with one axle.

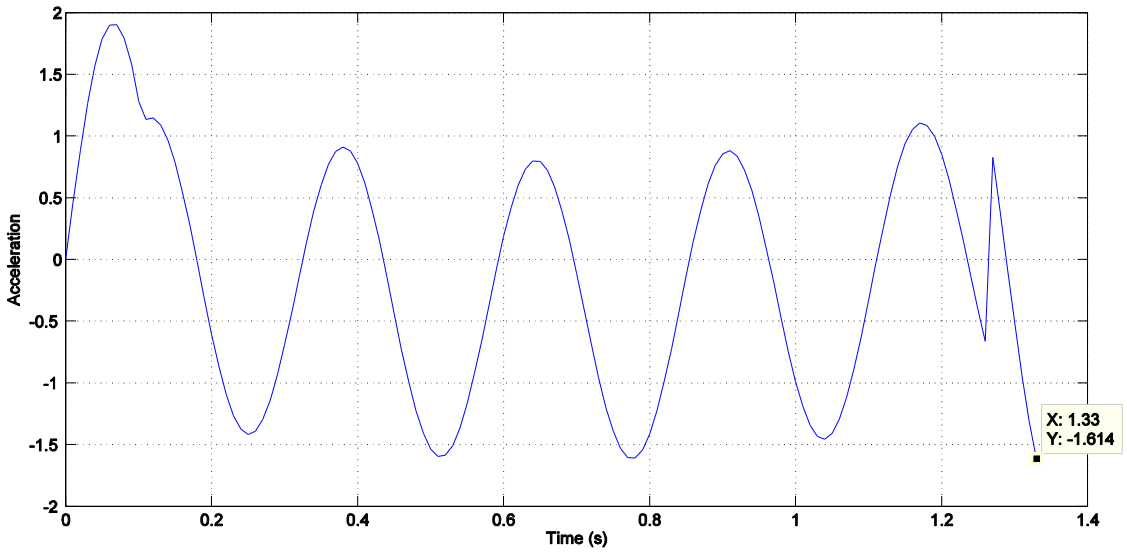

Figure 3.12 Acceleration at mid-span of the bridge with $c = 88 km/h$

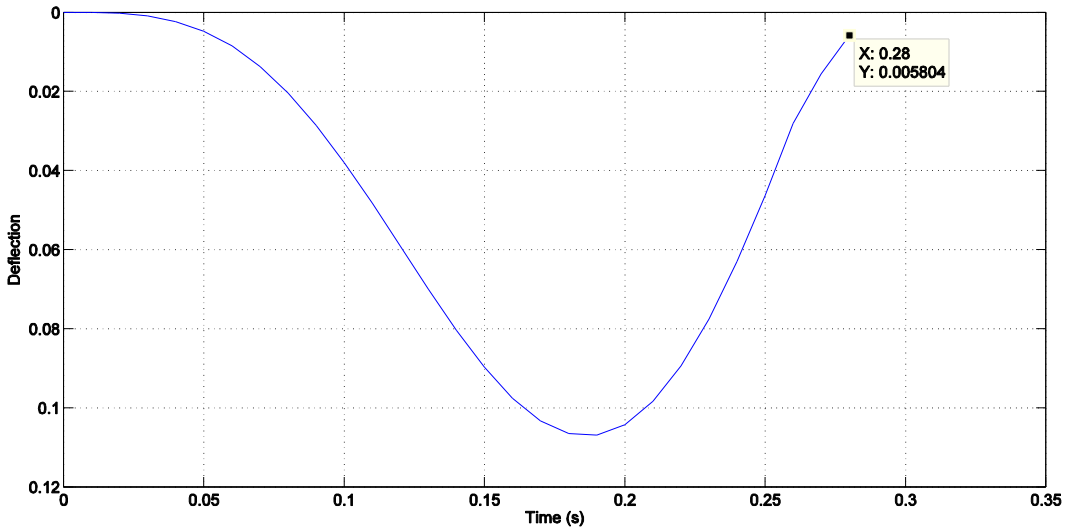

Figure 3.13 Dynamic deflection at mid-span of the bridge with $c = 410\,km/h$

From the above figure we can note that the front axle of the truck enters the bridge at 0 seconds and the rear axle exits at 0.28 seconds, which is 0.02 seconds more than the vehicle with one axle moving at the same speed (Figure 3.3). The maximum deflection is also more because of the added weight of the second axle.

Figure 3.8 is the acceleration plot of the truck with two axles moving at a very high speed of 410 km/h.

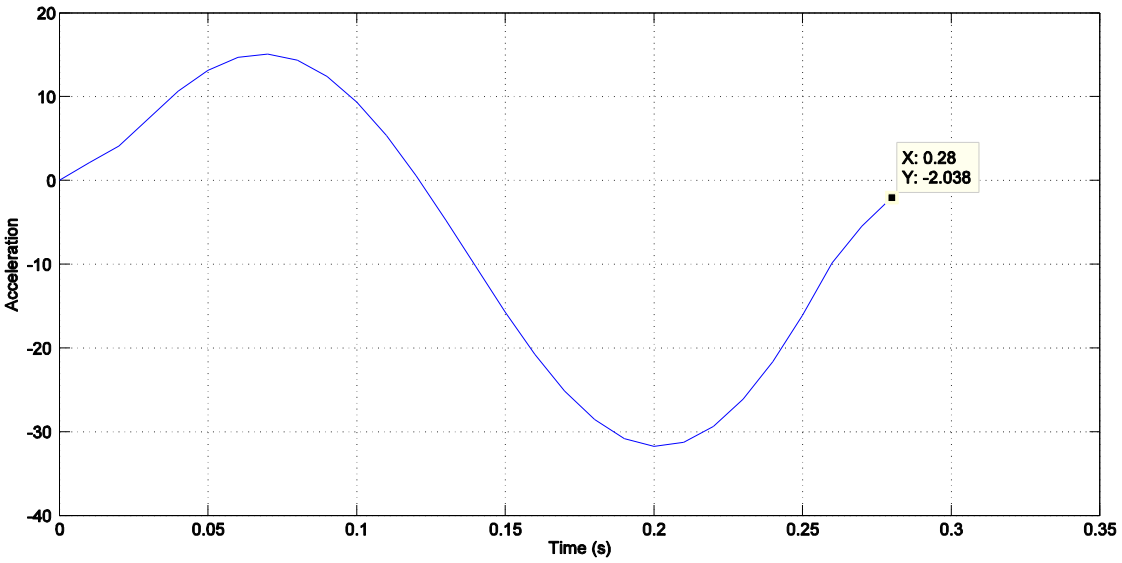

Figure 3.14 Acceleration at mid-span of the bridge with $c = 410\,km/h$

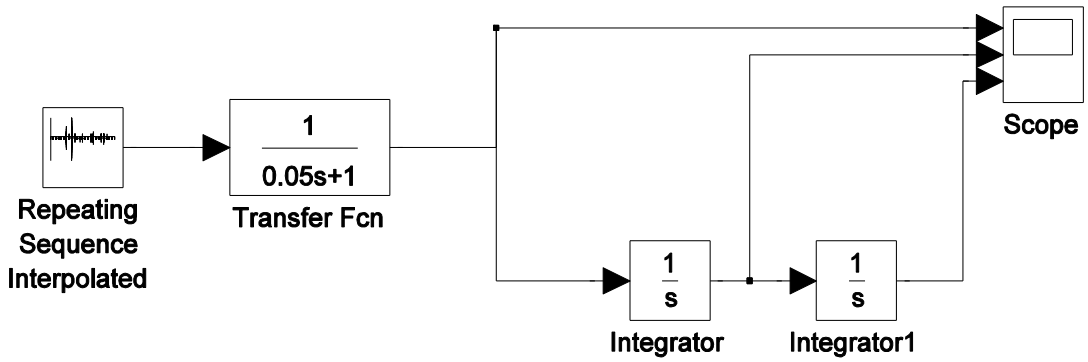

Figure 3.15 Simulink Block Diagram setup for generating displacement and velocity from noise filtered acceleration measurements.

3.3 Comparison with real time data

In this section we compare the results of the analysis in the previous sections to response data collected from the Canadian River Bridge. The data is quite noisy so it was filtered by a low pass filter with bandwidth 100 rad/sec to remove most of the noise. The measured acceleration data was integrated to obtain the bridge velocity and displacement. The data used in this analysis was

received from a single sensor on the Canadian River Bridge located at the center of the bridge. We used the Simulink model shown in Figure 3.9 to generate the velocity and deflection.

A small bit of data of 2 seconds was selected because it takes less than 2 minutes for a vehicle to cross the bridge section on a highway. The output of the scope is shown in Figure 3.10. We note that the periodic notation of the top plot is acceleration with a length of 2 seconds is taken, which represents the response data from a single vehicle travelling at 88 km/h.

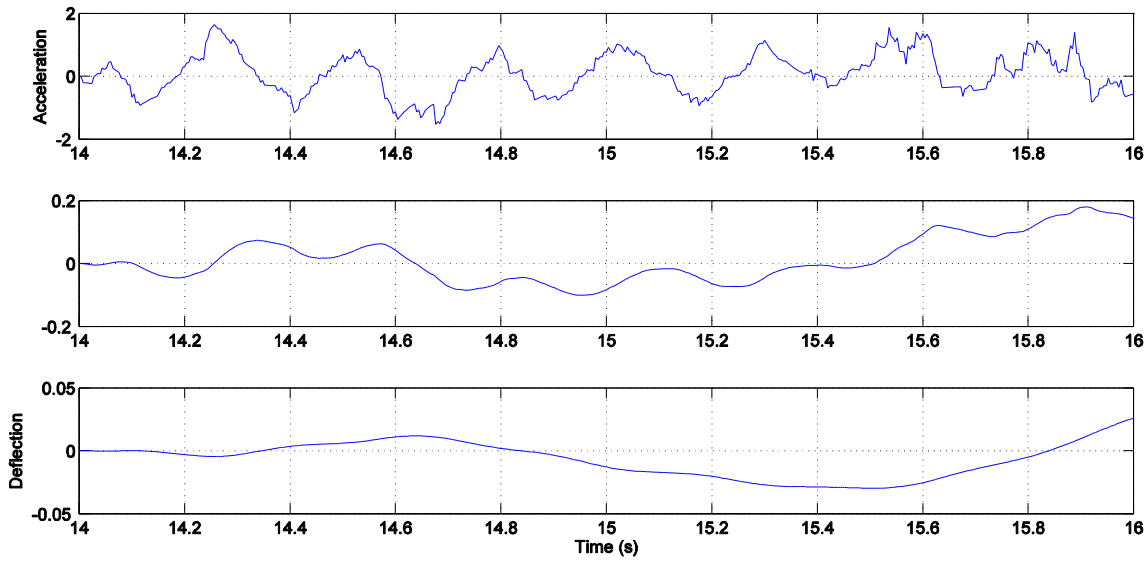

Figure 3.16 Snapshot of Scope showing vertical deflection, velocity and acceleration from 14 to 16 seconds

We note that the acceleration plot is approximately periodic and is similar to Figure 3.6 although Figure 3.10 is considerably more noisy. The bottom plot is the bridge deflection. Again, we note that, the plot is similar to deflection plot in Figure 3.5.

Chapter 4: Identification of Vehicle Load

Bridge sensor network measures the combined response of the bridge and load, i.e. the system is outlined in Figure 2.3. If a perfect bridge model is available then, in principle, the load can be reconstructed by an inversion of the bridge model. However, such a problem is not well posed. Therefore, we developed an algorithm that is based on an

approximate inverse operation. Furthermore, for real time computational and robustness purposes, we employ a reduced order physics based Gray Box model of the bridge such as the one derived in Section 3.1. For robustness and stability purposes we employed the feedback structure shown in Figure 4.1.

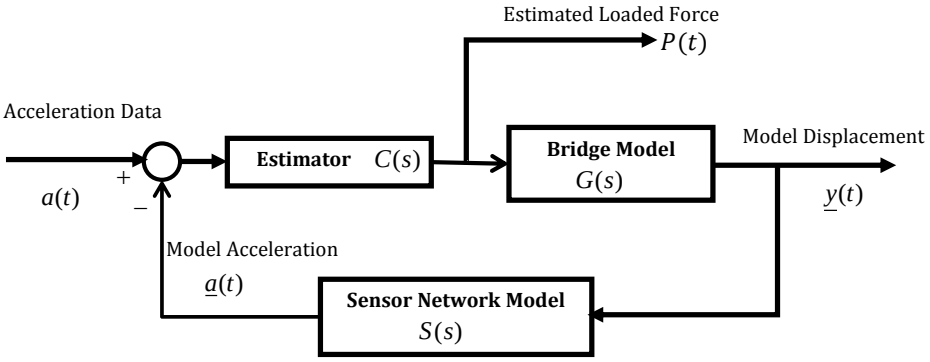

Figure 4.17 Functional Layout for the Closed Loop Load Estimation Algorithm: G(s) is the bridge model transfer function and S(s) is a sensor transfer function. The estimator produces the load force using the error between the real acceleration and the model generated acceleration.

Let $G(s)$ be the reduced order (or full order) bridge model and let $S(s)$ be the sensor transfer function. Here the transfer function $G(s)$ represents the Laplace transform of the impulse response of the bridge model. The estimator block $C(s)$ is a design parameter to be determined. The input to the system is the measured acceleration $a(t)$, which is the true vertical acceleration of the bridge deck obtained from the sensor network, plus measurement noise. We assume that the data is preprocessed (filtered) to remove the high frequency of the measurement noise. The output of the feedback loop is the estimated or reconstructed acceleration $\underline{a}(t)$. The transfer function between the acceleration input $a(t)$ and output $\underline{a}(t)$ of the closed loop system in Figure 4.1 is

$$T(s) = \frac{C(s)G(s)S(s)}{1 + C(s)G(s)S(s)} \qquad (0.0)$$

Let $H(s) = G(s)C(s)$ then

$$T(s) = \frac{C(s)H(s)}{1 + C(s)H(s)} \qquad (0.0)$$

Ideally one would like to make $T(s)$ equal to 1 in which case $\underline{a}(t) = a(t)$ and the input $P(t)$ to $G(s)$ is the load input to the bridge (provided certain stability and other technical conditions are met). However, obviously this objective can never be met, i.e. an Estimator $C(s)$ that could meet this objective would be infinitely large. We note however that it is possible to make $T(s)$ approximately equal to unity for all (low) frequencies of interest, i.e. if we let $[0,100]$ be the frequency band (bandwidth of the bridge) of the interest we want to select $C(s)$ such that $T(j\omega) \approx 1$ for $\omega \in [0,100]$, i.e. $|T(j\omega)| \approx 1$ and $\angle(j\omega) \approx 0, \omega \in [0,100]$. Note that $T(j\omega)$ is the frequency response of the system evaluated at $s = j\omega$. We designed an Estimator $C(s)$ that satisfies these constraints using the H_∞ control technique discussed in Section 2.2.

5.1 Estimator design

The estimator $C(s)$ shown in Figure 4.1, was designed using H-infinity techniques. The objective is to obtain $T(j\omega) \approx 1$ for $\omega \in [0,100]$, i.e. $|T(j\omega)| \approx 0$ and $\bar{\sigma}(j\omega) \approx 0,\ \omega \in [0,100]$. The first step in the design process is to select the approximate weighting functions W_e, W_u and W_y and in this case, we need $S = (1+CH)^{-1}$ small over a desired frequency range i.e. $1+CH$ is large but we already know that H is small, so we have to pick W_e such that C is large and constant over the desired frequency range. Using trial and error methods the weighting functions picked are

$$\begin{aligned} W_e &= 10^6 \frac{s+5000}{s+500} \\ W_u &= 10^{-6} \\ W_y &= 0 \end{aligned} \qquad (0.0)$$

We can notice that W_e is of the form (2.6) and since C is large $T = CH/1+CH \approx 1$, so we don't need W_y in this case and to satisfy (2.4) which is $\|W_u C/1+CH\| < 1$ we consider $W_u = 10^{-6}$.

After selecting the weighting functions, the estimator $C(s)$ is designed using the H-infinity control technique which gave us the desired closed loop response and at the same time resulted in a stable control signal output, i.e. the transfer function from $a(t)$ to $P(t)$ is stable. The optimal estimator has the following transfer function.

$$C(s) = \frac{.4522s^4 + 904.7s^3 + 453100s^2 + 921900s + 2582\times10^5}{10^{-16}s^5 + 1.418\times10^{-9}s^4 + 1.006\times10^{-2}s^3 + 5.036s^2 + 3.692s + 5.187\times10^{-2}} \qquad (0.0)$$

The transfer function of the bridge given by (3.6) with $\omega_{(1)} = 23.8768$ rad/sec, $\omega_b = 0.375$ rad/sec and $\mu = 10^4$ is given below

$$H(s) = \frac{10^{-4} s^2}{s^2 + 0.75s + 570.1} \qquad (0.0)$$

Figure 5.1, shows the bode plot of the open loop transfer function, we note the low DC gain and large resonant peak at $\omega_{(1)} = 23.8768$ rad/sec. Furthermore, there is a sharp change in phase around the corner frequency.

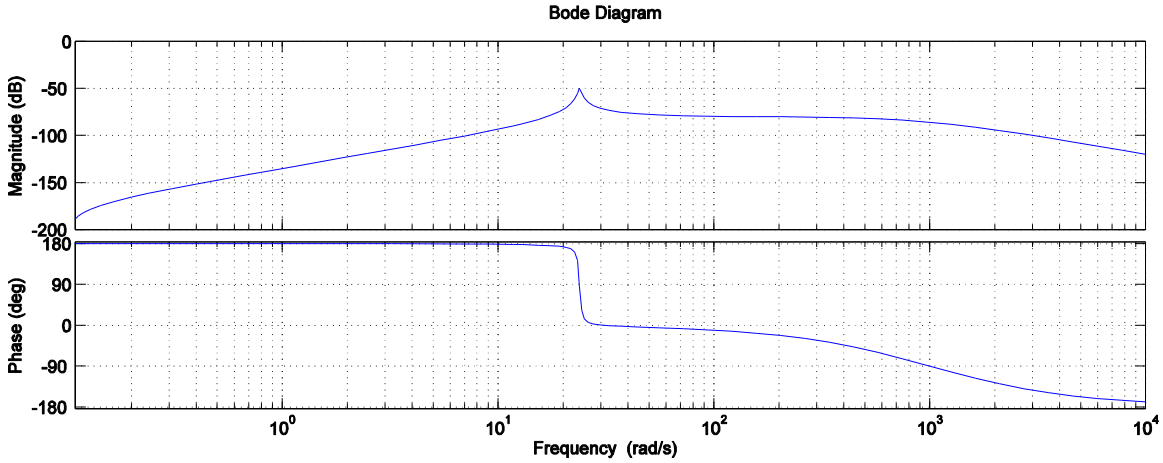

Figure 5.18 Bode Plot of the open loop bridge transfer function frequency response.

5.1.1 Closed loop transfer function of the system

The closed loop transfer function $T(s)$ is expected to be close to 1 over the frequency of interest $0-100\ rad/s$. The bode plot of $T(s)$ is shown in Figure 5.2

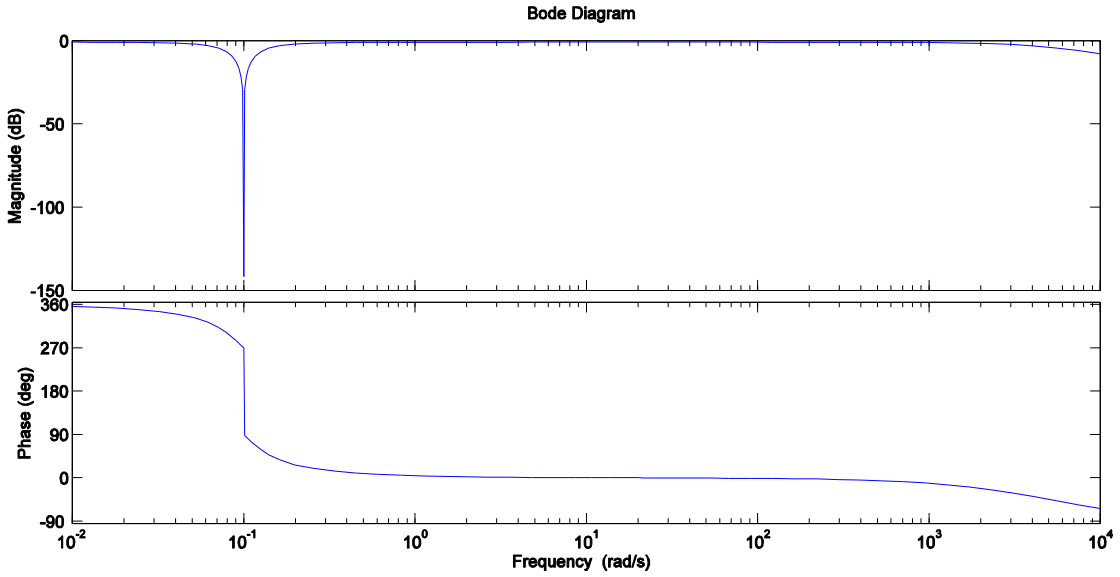

Figure 5.19 Bode plot of the closed loop transfer function frequency response.

From the above figure we note that $|T(j\omega)|$ is indeed approximately equal to 0 which implies $T(j\omega)$ is approximately equal to 1 over the frequency range of interest. Furthermore, the phase is close to 0 degrees over the same frequency range. It can be seen in the Figure 5.3 which is the bode plot of the closed loop transfer function.

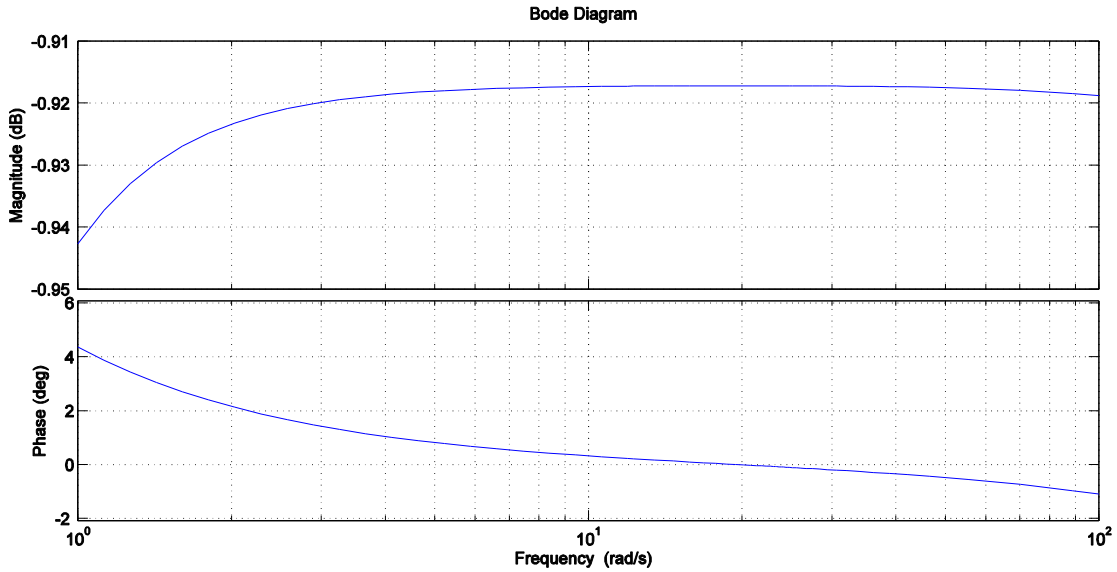

Figure 5.20 Bode plot of closed loop transfer function over frequency of interest

5.1.2 Closed loop transfer function of the Estimator

The closed loop transfer function from the acceleration input to the output of the Estimator is

$$R(s) = \frac{C(s)}{1 + C(s)H(s)} \qquad (0.0)$$

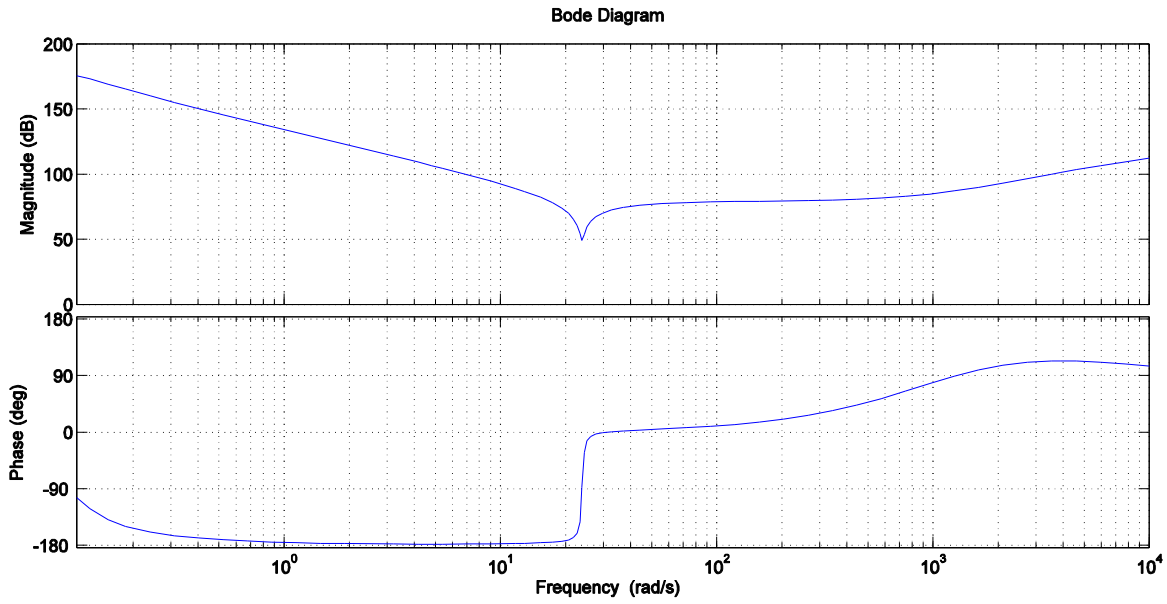

Figure 5.21 Bode plot of the closed loop transfer function of the estimator frequency response.

The above figure is the bode plot of the closed loop transfer function of the estimator, we note that high gain and a dip in the magnitude and a sharp change in phase at the corner frequency ω_1.

5.2 Performance of the Closed loop system

As discussed earlier in Chapter 4 we would like to have $T(s)$ approximately equal to 1, which implies $a(t) \approx \underline{a}(t)$. In this section we compare the input-output behavior of the closed loop system. We use idealized acceleration data from the model in Section 3.1 as well as real data.

5.2.1 Performance using Acceleration from (3.8)

Recall (3.8)

$$a\left(\frac{l}{2},t\right)=v_0\frac{1}{1-\alpha^2}\left(\omega^2\sin\omega t-\alpha\omega_1^2\sin\omega_1 t\right) \qquad (0.0)$$

If we pass the above signal through the system with the different speeds used before, which are $c=88\,km/h$ (Critical speed on the bridge) and $c=410\,km/h$ (Very high speed) with respective α values 0.108, 0.5, we get the responses shown in Figures 5.5 and 5.6. In these plots the system input is blue in color, the system output is red in color and the estimator output is orange in color for $c=88,\,410\,km/h$ or $\alpha=0.108\,\&\,0.5$ respectively.

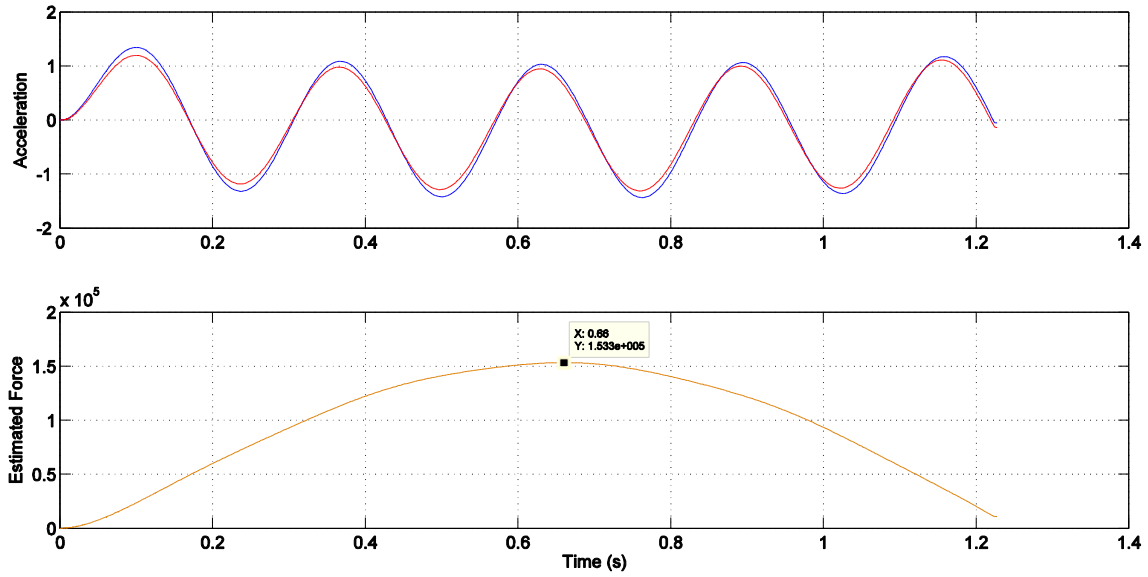

Figure 5.22 System Response for c=88 km/h. The top plot shows the real (input) and model generated acceleration while the bottom plot shows the force predicted by the Estimator.

From Figure 5.5, we can note that the vehicle axle enter the bridge at 0 seconds and leave at 1.22 seconds when it is traveling with a speed of 88 km/h. We can see that the estimated load force is 153300 Newton's and from the estimated force we can calculate the

weight of the vehicle which will be 15643 Kg which is very close to the value we assumed to calculate v_0 in Chapter 3.

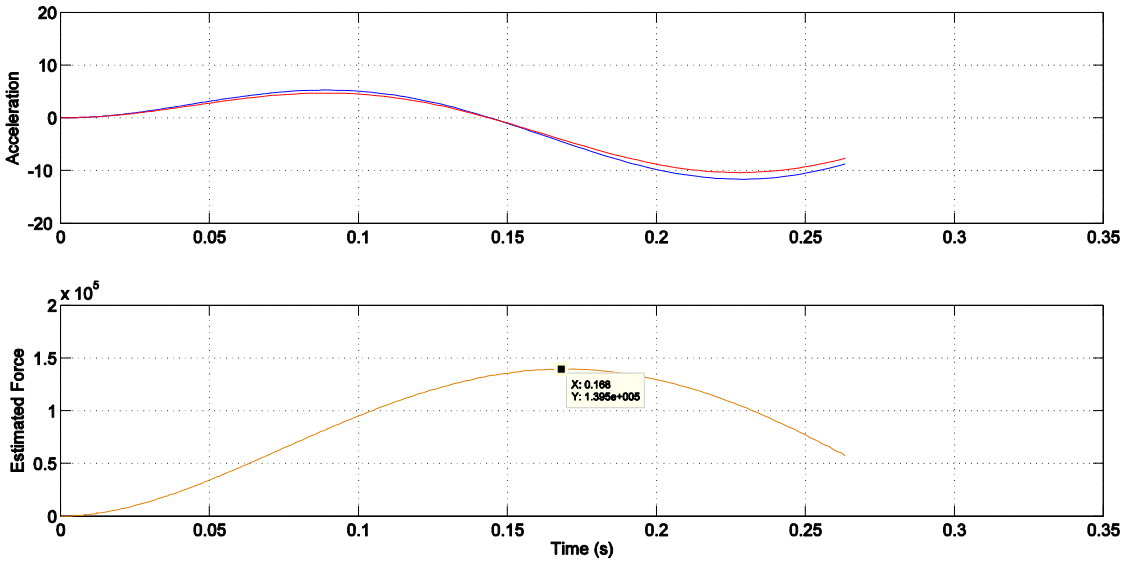

Figure 5.23 System Response for c=410 km/h. The top plot shows the real (input) and model generated acceleration while the bottom plot shows the force predicted by the Estimator.

Figure 5.6, gives us the system response when the input is the acceleration of a vehicle moving at a speed of 410 km/h. From the above Figure we can note that the estimated force is 139500 Newton so the weight of the vehicle will be 14235Kg, even though the vehicle is moving at a very high speed the estimated weight of the vehicle is pretty much close to the vehicle travelling at a speed of $c = 88 km/h$.

5.2.2 Performance using Real time data

In Figure 5.7, we compare the system response using real time data. As we discussed earlier in Section 2.5, each span is of 30 meters in length. The Sensor network is located only in three spans of the bridge. Considering the average length and speed of the vehicle, we can say that every vehicle takes approximately 2 seconds to cross the sensor network. Here we use a 2 second window of 14 to 16 seconds.

Figures 5.7 and 5.8, are the times response of the input and output of the system. In these plots, the blue colored plot is the input data collected from the Canadian River Bridge (Acceleration Data) and the red colored plot is the output of the closed loop system (Modal Acceleration). We can notice that they overlap each other, so we can say $a(t) \approx \underline{a}(t)$

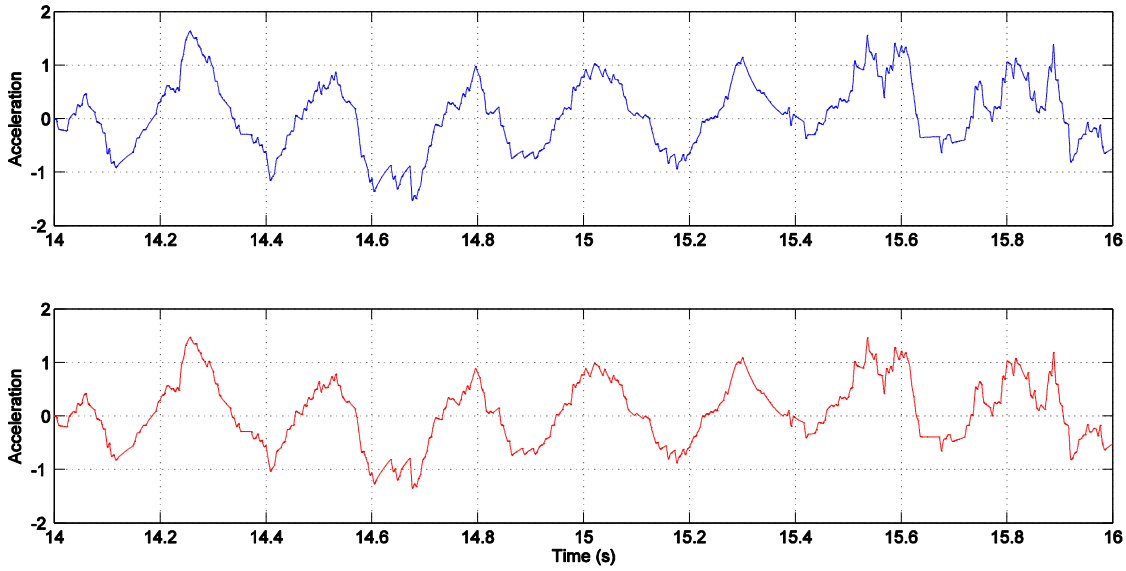

Figure 5.24 Time response of input and output of the system. Top plot shows the real acceleration measurements while the bottom plot shows the corresponding model generated acceleration from the load estimation algorithm.

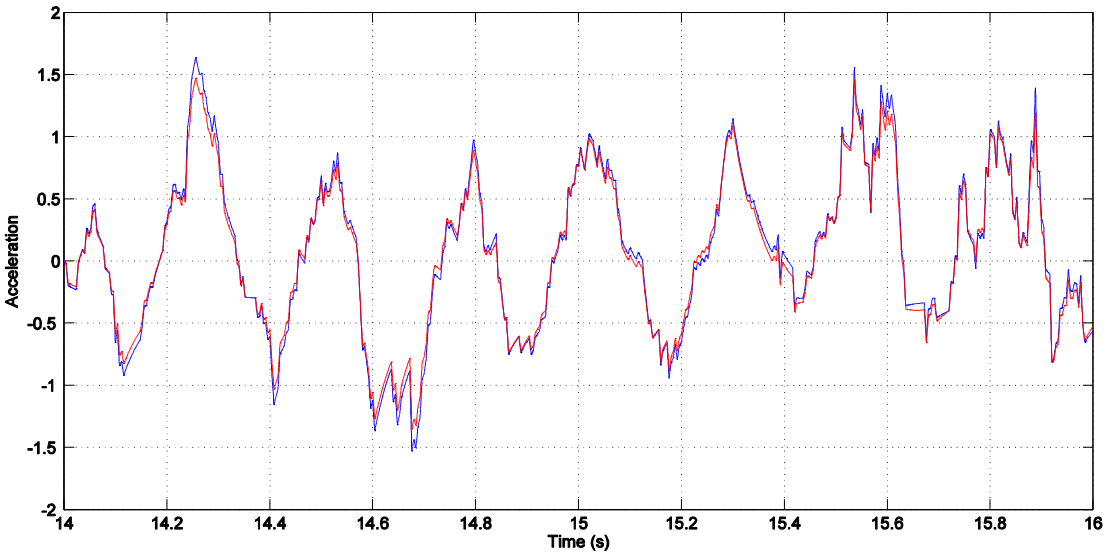

Figure 5.25 Time response of the measured and estimator algorithm generated accelerations in the same plot.

Now let's look at the same 2 second window in Figure 5.9, where the first plot in the subplot is the output of the system overlapped on the input and the second plot is the output of the estimator.

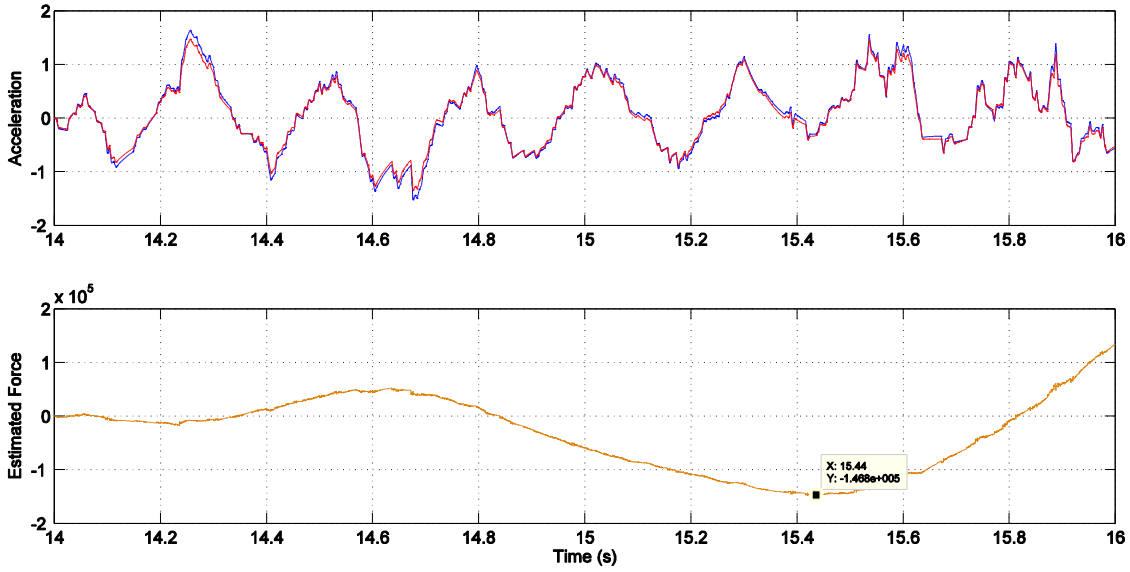

Figure 5.26 Acceleration and Force plots. The top plot shows the measured and model generated acceleration signals and the bottom plot shows the load force generated by the closed loop load estimation algorithm.

When we take a look at the force which is estimated to be 1.468×10^5 Newton, so the mass of the vehicle will be 14,980 Kg.

5.3 Robustness of the Solution

To determine the ability of the system to resist change in the bridge parameters like ω_b, μ and $\omega_{(1)}$, we calculate the sensitivity functions of the closed loop transfer function. Recall that the closed loop transfer function is

$$T(s)=\frac{C(s)G(s)S(s)}{1+C(s)G(s)S(s)} \qquad (0.0)$$

Since $C(s)$ and $S(s)$ do not depend on ω_b, μ and $\omega_{(1)}$, for simplicity let $\hat{C}(s)=C(s)S(s)$

5.3.1 Sensitivity function with respect to ω_b

The sensitivity function of the closed loop transfer function with respect to ω_b is

$$S_{\omega_b}^{T} = \frac{\partial T}{\partial \omega_b}\frac{\omega_b}{T}$$

$$\frac{\partial T}{\partial \omega_b}\frac{\omega_b}{T} = \left(\frac{\left(1+\hat{C}G\right)C\frac{\partial G}{\partial \omega_b}}{\left(1+\hat{C}G\right)^2} - \frac{\left(\hat{C}G\right)\hat{C}\frac{\partial G}{\partial \omega_b}}{\left(1+\hat{C}G\right)^2}\right)\frac{\left(1+\hat{C}G\right)\omega_b}{\hat{C}G}$$

$$= \frac{\hat{C}\frac{\partial G}{\partial \omega_b} + \hat{C}^2 G\frac{\partial G}{\partial \omega_b} - \hat{C}^2 G\frac{\partial G}{\partial \omega_b}}{\left(1+\hat{C}G\right)^2}\frac{\left(1+\hat{C}G\right)\omega_b}{\hat{C}G}$$

$$= \frac{\hat{C}\frac{\partial G}{\partial \omega_b}}{\left(1+\hat{C}G\right)}\frac{\omega_b}{\hat{C}G}$$

$$\begin{aligned}
&= \frac{\omega_b}{G(1+\hat{C}G)}\frac{\partial G}{\partial \omega_b} \\
&= \frac{\omega_b}{G(1+\hat{C}G)}\frac{-2s/\mu}{\left(s^2+2\omega_b s+\omega_{(1)}^2\right)^2} \\
&= \frac{\omega_b}{G(1+\hat{C}G)}\frac{-2s}{\left(s^2+2\omega_b s+\omega_{(1)}^2\right)}G \\
&= \frac{1}{(1+\hat{C}G)}\frac{-2s\omega_b}{\left(s^2+2\omega_b s+\omega_{(1)}^2\right)}
\end{aligned} \qquad (0.0)$$

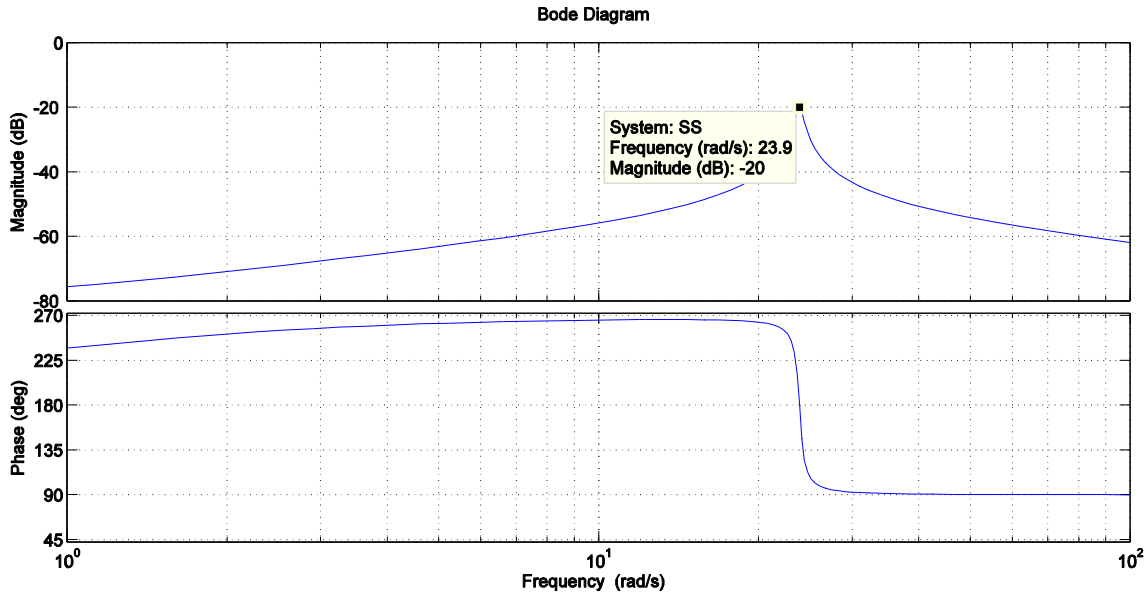

Figure 5.27 Bode plot of Sensitivity function with respect to bridge damping ω_b

The above Figure is the bode plot of sensitivity function with respect to ω_b and we can note that it has a low gain.

5.3.2 Sensitivity function with respect to μ

The sensitivity function of the closed loop transfer function with respect to μ is

$$S_{\mu}^{T} = \frac{\partial T}{\partial \mu}\frac{\mu}{T}$$

$$\frac{\partial T}{\partial \mu}\frac{\mu}{T} = \left(\frac{\left(1+\hat{C}G\right)C\frac{\partial G}{\partial \mu}}{\left(1+\hat{C}G\right)^2} - \frac{\left(\hat{C}G\right)\hat{C}\frac{\partial G}{\partial \mu}}{\left(1+\hat{C}G\right)^2} \right) \frac{\left(1+\hat{C}G\right)\mu}{\hat{C}G}$$

$$= \frac{\hat{C}\frac{\partial G}{\partial \mu} + \hat{C}^2 G\frac{\partial G}{\partial \mu} - \hat{C}^2 G\frac{\partial G}{\partial \mu}}{\left(1+\hat{C}G\right)^2} \frac{\left(1+\hat{C}G\right)\mu}{\hat{C}G}$$

$$= \frac{\hat{C}\frac{\partial G}{\partial \mu}}{\left(1+\hat{C}G\right)} \frac{\mu}{\hat{C}G}$$

$$= \frac{\mu}{G(1+\hat{C}G)} \frac{\partial G}{\partial \mu}$$

$$= \frac{\mu}{G(1+\hat{C}G)} \frac{-\left(s^2+2\omega_b s+\omega_{(1)}^2\right)/\mu^2}{\left(s^2+2\omega_b s+\omega_{(1)}^2\right)^2}$$

$$= \frac{-1}{(1+\hat{C}G)} \qquad (0.0)$$

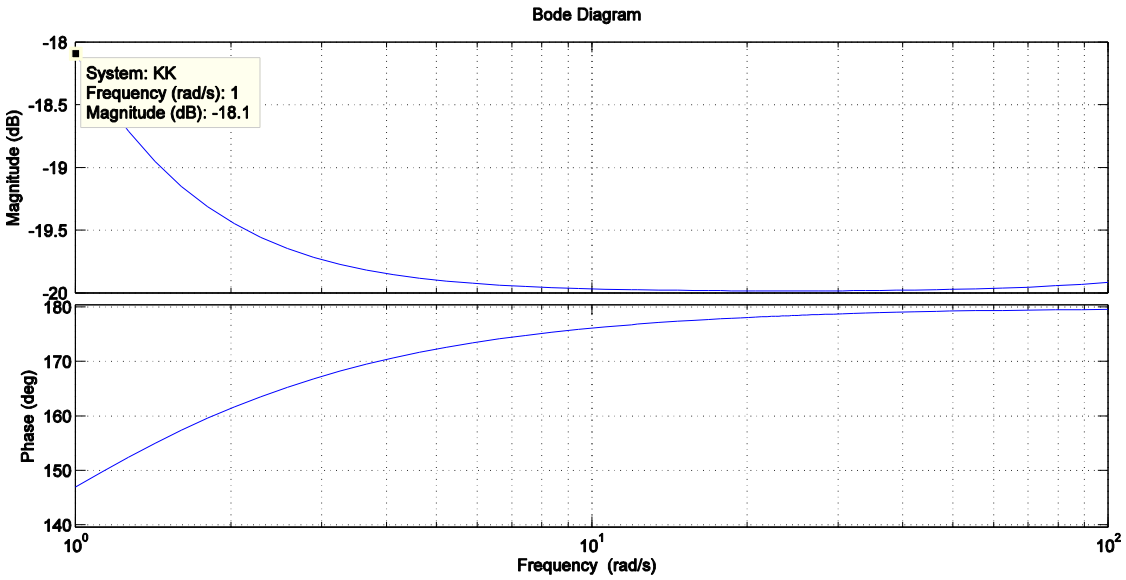

Figure 5.28 Bode plot of Sensitivity function with respect to bridge mass μ

Figure 5.11 is the bode plot of the sensitivity function with respect to μ which also have a low gain

5.3.3 Sensitivity function with respect to $\omega_{(1)}$

The sensitivity function of the closed loop transfer function with respect to $\omega_{(1)}$ is

$$S^{T}_{\omega_{(1)}} = \frac{\partial T}{\partial \omega_{(1)}} \frac{\omega_{(1)}}{T}$$

$$\frac{\partial T}{\partial \omega_{(1)}} \frac{\omega_{(1)}}{T} = \left(\frac{\left(1+\hat{C}G\right) C \frac{\partial G}{\partial \omega_{(1)}}}{\left(1+\hat{C}G\right)^2} - \frac{\left(\hat{C}G\right)\hat{C} \frac{\partial G}{\partial \omega_{(1)}}}{\left(1+\hat{C}G\right)^2} \right) \frac{\left(1+\hat{C}G\right)\omega_{(1)}}{\hat{C}G}$$

$$= \frac{\hat{C} \frac{\partial G}{\partial \omega_{(1)}} + \hat{C}^2 G \frac{\partial G}{\partial \omega_{(1)}} - \hat{C}^2 G \frac{\partial G}{\partial \omega_{(1)}}}{\left(1+\hat{C}G\right)^2} \frac{\left(1+\hat{C}G\right)\omega_{(1)}}{\hat{C}G}$$

$$= \frac{\hat{C} \frac{\partial G}{\partial \omega_{(1)}}}{\left(1+\hat{C}G\right)} \frac{\omega_{(1)}}{\hat{C}G}$$

$$= \frac{\omega_{(1)}}{G(1+\hat{C}G)} \frac{\partial G}{\partial \omega_{(1)}}$$

$$= \frac{\omega_{(1)}}{G(1+\hat{C}G)} \frac{-2\omega_{(1)}/\mu}{\left(s^2 + 2\omega_b s + \omega_{(1)}^2\right)^2}$$

$$= \frac{-2\omega_{(1)}^2}{(1+\hat{C}G)} \frac{1}{\left(s^2 + 2\omega_b s + \omega_{(1)}^2\right)} \qquad (0.0)$$

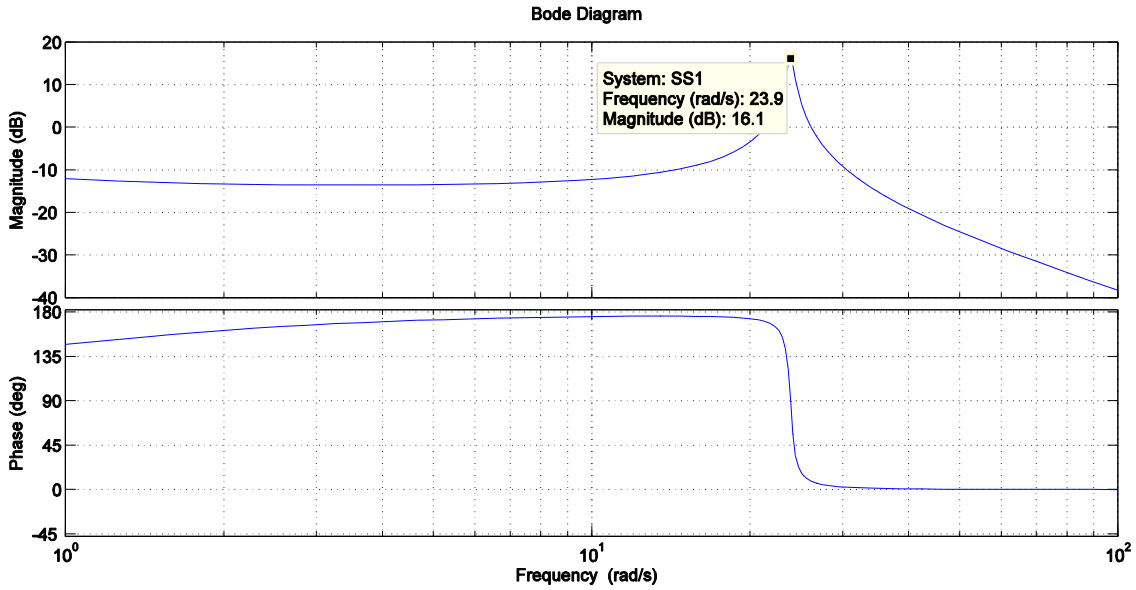

Figure 5.29 Bode plot of Sensitivity function with respect to fundamental mode $\omega_{(1)}$

Figure 5.12 is the bode plot of the sensitivity function with respect to $\omega_{(1)}$ which has a high gain when compared to sensitivity function with respect to ω_b and μ.

To calculate the variation we can have in ω_b, μ and $\omega_{(1)}$ so that we get 10% accuracy in the force, we need the maximum gains of the sensitivity functions with respect to ω_b, μ and $\omega_{(1)}$. From Figures 5.10, 5.11 and 5.12 maximum gain of the sensitivity functions are equal to $-20dB$, $-18.1dB$ and $16.1dB$ respectively.

$$\frac{\partial T}{\partial \omega_b}\frac{\omega_b}{T} \leq K_1 \qquad (0.0)$$

$$\frac{\partial \omega_b}{\omega_b} \geq \frac{\partial T}{TK_1} \qquad (0.0)$$

$$\frac{\partial \omega_b}{\omega_b} \geq \frac{0.1}{0.1} = 1 \qquad (0.0)$$

Therefore 100% variation can be allowed to get 10% of accuracy in the force

Similarly

$$\frac{\partial T}{\partial \mu}\frac{\mu}{T} = K_2$$

$$\frac{\partial \mu}{\mu} = \frac{\partial T}{TK_2} \qquad (0.0)$$

$$\frac{\partial \mu}{\mu} = \frac{0.1}{0.1245} = 0.8032 \qquad (0.0)$$

To get 10% of accuracy in the force 80% of variation in μ can be allowed

Similarly

$$\frac{\partial T}{\partial \omega_{(1)}}\frac{\omega_{(1)}}{T} = K_3$$

$$\frac{\partial \omega_{(1)}}{\omega_{(1)}} = \frac{\partial T}{TK_3}$$

$$\frac{\partial \omega_{(1)}}{\omega_{(1)}} = \frac{0.1}{6.3826} = 0.0157 \qquad (0.0)$$

To get 10% of accuracy in the force only 1.57% of variation in $\omega_{(1)}$ can be allowed between the frequencies 20 rad/sec and 30 rad/sec, But other than these frequencies sensitivity of the closed loop transfer function is very less.

From the above results we can note that 100 percentage of variation in circular frequency of damping of the bridge is allowed and approximately 80 percentage of variation in constant mass per unit length of the bridge is allowed but not much of

variation is allowed in the central frequency of fundamental mode of vibration of the bridge in between a small frequency range.

Chapter 6: Concluding Remarks and Future Work

In this report, we present a technique for a data driven real time estimation of the dynamic loads on the bridge generated by passing vehicles. We developed an approach where no dynamic modal of the load is required and the load of the vehicle is estimated directly. In the process of estimating input load, we developed an estimator using feedback control methods to reconstruct the vehicle load by comparison of the measured bridge response and model response. The estimator output gives the input to the bridge model, which is the estimated load force that can be used to estimate the load of the vehicle. We also evaluated the robustness of the approach against variations in the bridge parameters.

Future work is needed to implement the developed approach in real time software as well as field tests.

References

[1] B.A. Francis. *Lecture Notes in Control and Information Sciences*, Springer–Verlag, Berlin, Heidelberg 1997.

[2] S. Nourazari. *Identification of Dynamic Structural Loads*, MS Thesis: University of Oklahoma, Norman, OK, 2009.

[3] T.H.T. Chan, L.Yu, S.S. Law, and T.H. Yung. "Moving Force Identification Studies, I: Theory," *Journal of Sound and Vibration*, Vol. 247, pp. 59-76, 2001.

[4] S.W. Doebling, C.R. Farrar,M. B. Prime, and D.W. Shevitz, *Research Report LA-103070-MS, ESA-EA: Identification and Health Monitoring of Structural and Mechanical Systems from Changes in Their Vibration Characteristics: A Literature Review*, Los Alamos National Laboratory, Los Alamos, NM, USA, 1996.

[5] L. Fryba. *Vibration of Solids and Structures under Moving Load*, 3rd Edition, Thomas Telford, London, 1999.

[6] G.W. Housner, L.A. Bergman, T.K. Caughey, A.G. Chassiakos, R.O. Claus, S.F. Masari, R.E. Skelton, T.T Soong, B.F. Spencer B.F., and J.T.P. Yao. "Structural Control: Past, Present and Future," *Journal of Engineering Mechanics*, Vol. 123, pp. 897-971, 1997.

[7] A.N. Krylov, "Uber die erzwungenen schwingungen von gleichformingen ealstischen staben," *Mathematical Collection of Papers of the Academy Sciences*, Vol. 61 pp. 211, 1905.

[8] L. Meyyappan, M. Jose, C. Dagali, P. *Silva and H. Pottinger, "Fuzzy- neuro system of bridge health monitoring," Proceedings of 22nd International Conference of the North American Fuzzy Information Processing Society*, pp. 8-13, 2003.

[9] T.P. Nordberg and I. Gustafsson, "Dynamic regularization of input estimation problems by explicit block inversion," *Comput. Methods Appl. Mech. Engrg*, Vol. 195 pp. 5877-5890, 2006.

[10] B. Peeters, *System Identification and Damage Detection in Civil Engineering*, PhD Thesis, Katheolieke University Leuven, Leuven, Belgium, 2000.

[11] Structural Vibration Solutions A/S, *ARTeMIS Extractor Pro*, http://www.svibs.com/products/extractor.htm, 2009.

[12] A.D. Stelzner, D.C. Kammer, and P. Milenkovic. "A time domain method for estimating forces applied to an unrestrained structure," *Transactions of the ASME*, Vol. 123, pp. 524-532, 2001.

[13] A. Teughels and G. De Roeck, "Structural Damage Identification of the Highway Bridge Z24 by FE Model Updating," *Journal of Sound and Vibration*, Vol. 278, pp. 589-610, 2004.

[14] A. Lanzon, X. Bombois and B.D.O. Anderson. "On weight adjustments in H-infinity Control design", *Proceedings of the European Control Conference EEC 03*, pp. 227-231, 2003.

[15] P. Benner R.W. Freund, D.C Sorensen, and A. Varga (eds), *Linear Algebra and its Applications: Special issue on Order reduction of Large-scale Systems*, Vol. 415, 2006.

[16] E.B. Rudnyi and J.G. Korvink. "Model Order Reduction for Large Scale Engineering Models Developed in ANSYS," *Lecture notes in Computer Science*, Vol. 3723, pp. 349-356, 2006.

[17] J. Hu and C. Bohn, H.R. Wu. "Systematic H-infinity Weighting Function Selection and its Application to the Real-time Control of a Vertical Take-off Aircraft," *Control Engineering Practice*, Vol. 8, pp. 241-252, 2000.

[18] D. McFarlane and K. Glover. "A Loop Shaping Design Procedure Using H-infinity Synthesis", *IEEE Trans Automat Contr*, Vol. 37, pp. 759-769, 1992.

[19] I. Postlethwaite, S.D. O'Young, D.W. Gu and J. Hope, "H-infinity Control System Design: A Critical Assessment Based on Industrial Applications," *Proceedings of IFAC 10 World Congress on Automatic Control*, pp. 328-333, Munich, 1987.

[20] AASHTO, *AASHTO LRFD Bridge Design Specifications*, 3rd Edition. Washington DC, 2004.

[21] K. Zhou, J.C. Doyle and K. Glover. *Robust and Optimal Control*, Prentice Hall, Upper Saddle River, NJ, 1995.

[22] L. Ljung, *System Identification: Theory for the user*, Second Edition", Prentice Hall, Upper Saddle River, NJ, 1999.

[23] A.C. Antoulas, "Approximation of linear dynamical systems;" *Wiley Encyclopedia of Electrical and Electronics Engineering*, Edited by J.G. Webster", pp. 403-422, 1999.

[24] G. Goodwin, *Control System Design*, Prentice Hall, Upper Saddle River, NJ, 2001.

[25] R.K. Gupta and R.W.Traill-Nash, "Bridge Dynamic Loading Due to Road Surface Irregularities and Braking of Vehicle", *Earthquake Engineering and Structural Dynamics* Vol. 8, pp. 83-96, 1980.

[26] J.S. Wu, and C.W. Dai, "Dynamic Responses of Multi-span Non-uniform Beams due to Moving Loads", *Journal of Structural Engineering*, Vol. 113, pp. 458-474, 1987.

[27] T. Hayashikawa and N. Watanabe, "Dynamic Behavior of Continuous Beams with Moving Loads", *ASCE Journal of the Engineering Mechanics Division*, Vol. 107, pp. 229-246, 1981.

[28] J. Hu, C. Bohn and H.R. Wu, "Practical Approach to Selecting Weighting Functions for H-infinity Control and its Applications to a Pilot Plant", *UKACC International Conference on Control*, pp. 998-1003, UK, 1996.

[29] G.F. Franklin, D.J. Powell and M.L. Workman, *Digital Control of Dynamic Systems*, Addison Wesely, NY, 1990.

[30] S.S Nair, "Automatic Weight Selection Algorithm for Designing H Infinity Controller for Active Magnetic Bearing," *International Journal of Engineering Science and Technology*, Vol. 3, pp. 122-138, 2011.